THE UNIVERSITY OF MICHIGAN

COLLEGE OF ENGINEERING
DEPARTMENT OF ELECTRICAL ENGINEERING
Radiation Laboratory

Properties of the Triangular Lattice Array

By
DAVID H. S. CHENG

June 1968

Grant No. DA-AROD-31-124-G-724
Project No. 5638-E

Contract With: U. S. Army Research Office - Durham
Box CM, Duke Station
Durham, North Carolina 27706

Distribution of this document is unlimited.

Administered through:
OFFICE OF RESEARCH ADMINISTRATION • ANN ARBOR

PROPERTIES OF THE TRIANGULAR LATTICE ARRAY

David H. S. Cheng

The University of Michigan
Department of Electrical Engineering
The Radiation Laboratory
Ann Arbor, Michigan 48108

June 1968

Grant No. DA-ARO-D-31-124-G-724

Project No. 5638-E

Prepared for

U. S. Army Research Office - Durham
Box CM, Duke Station
Durham, North Carolina 27706

FOREWORD

This report, 7678-6-T, was prepared by The University of Michigan Radiation Laboratory, Department of Electrical Engineering, under the direction of Professor John A. M. Lyon and Professor Ralph E. Hiatt, on Army Grant No. DA-ARO-D-31-124-G-724 "Multi-Terminal Antenna Systems Study". The Grant is administered under the direction of the U. S. Army Research Office-Durham and the Contract Monitor is Dr. David B. vanHulsteyn

TABLE OF CONTENTS

I
INTRODUCTION

A new type of array consisting of elements arranged in a triangular lattice is studied in this report. The array has radiation characteristics similar to those of a tapered array but does not require tapered excitation.

A phased array of an arbitrary triangular lattice configuration is formulated using the vector model. It is applied to a special case of an isosceles triangular array.

The directivity of the array is derived and expressed in a compact form, whereby its enumeration becomes a routine procedure for any total number of elements. A general method of evaluating the mutual coupling terms involving two inclined short dipoles is developed.

Numerical results are presented and discussed as regards the radiation patterns and directivities of an isosceles triangular lattice array with its varying parameters such as the spacings between the adjacent elements and rows of elements, the phasings of the elements, and the size of the array.

II

RADIATION INTENSITY OF A TRIANGULAR LATTICE ARRAY OF DIPOLES

Let a planar triangular array of dipoles be situated in the x-y plane as shown in Fig. 1. The elements are identified by the lattice points spanned by the two base vectors, $\hat{a}_1$ and $\hat{a}_2$. The (m,n)'th dipole is located in the lattice by a vector $\hat{r}_{mn}=m\hat{a}_1+n\hat{a}_2$ drawn from the origin, where m, n are integers not exluding zero. The base vectors $\hat{a}_1$ and $\hat{a}_2$ are not necessarily equal or orthogonal, and are not, in general, of unit magnitudes. Since $\hat{a}_1$ axis is made to coincide with the x-axis, it can be shown that

$$\begin{aligned}\hat{a}_1&=a_1\hat{x}\\ \hat{a}_2&=a_2\cos\beta\,\hat{x}+a_2\sin\beta\,\hat{y}\end{aligned} \tag{1}$$

where β is the angle that $\hat{a}_2$ makes with $\hat{a}_1$. Hence, the lattice vector can also be expressed as

$$\hat{r}_{mn}=(ma_1+na_2\cos\beta)\hat{x}+na_2\sin\beta\,\hat{y} \quad . \tag{2}$$

The phase of the (m,n)'th element with respect to that of the elements at the origin is δ_{mn}

$$\delta_{mn}=m\delta_1+n\delta_2 \tag{3}$$

where δ_1 is the phase of any element relative to its immediate neighbor along the axis defined by the base vector $\hat{a}_1$ and δ_2 is defined similarly with respect to $\hat{a}_2$.

The contribution of (m,n)'th dipole in the array to the far field is

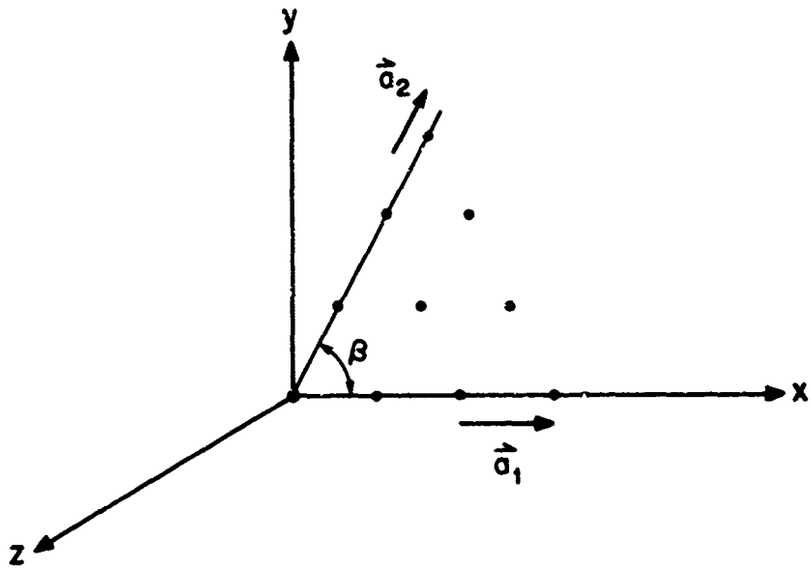

FIG. 1: TRIANGULAR LATTICE ARRAY

$$\vec{E}_{mn} = A_{mn} e^{j\delta_{mn}} \frac{e^{-jkR_{mn}}}{R_{mn}} \sin\theta_{mn} \hat{\theta}_{mn} \tag{4}$$

where A_{mn} is the excitation amplitude of the element, R_{mn} is the distance from the element to the point of observation, and $\sin\theta_{mn}\hat{\theta}_{mn}$ is the radiation vector of the dipole with respect to its own dipole moment. In terms of the spherical coordinates, the individual field can be expressed as

$$\vec{E}_{mn} = A_{mn} e^{j\delta_{mn}} \frac{e^{-jkR}}{R} e^{jkr_{mn}\cos(\phi-\phi_{mn})\sin\theta} \sin\theta_{mn}\hat{\theta}_{mn} . \tag{5}$$

The resultant field intensity is obtained by summing over the entire array

$$\vec{E} = \frac{e^{-jkR}}{R} \sum_{m=o}^{N-1} \sum_{n=o}^{N-m-1} A_{mn} e^{j\delta_{mn}} e^{jkr_{mn}\cos(\phi-\phi_{mn})\sin\theta} \sin\theta_{mn}\hat{\theta}_{mn} , \tag{6}$$

where N is the number of the elements along $\vec{a}_1$ or $\vec{a}_2$. By proper adjustment of amplitudes, spacing and phase in (6) a radiation pattern of almost any desired form can be obtained.

We shall consider only the case where all current amplitudes are the same and the base vectors $\vec{a}_1$, $\vec{a}_2$ define an isosceles triangular arrangement. Since $a_1 = a_2 = a$, it is found convenient to rotate the x-y plane counterclockwise about the z-axis through an angle α such that the new y' axis bisects the angle β_o as shown in Fig. 2. In terms of the x'-y' plane,

$$\begin{aligned} \vec{a}_1 &= a\cos\alpha\,\hat{x}' + a\sin\alpha\,\hat{y}' , \\ \vec{a}_2 &= a\cos(\alpha+\beta)\hat{x}' + a\sin(\alpha+\beta)\hat{y}' , \end{aligned} \tag{7}$$

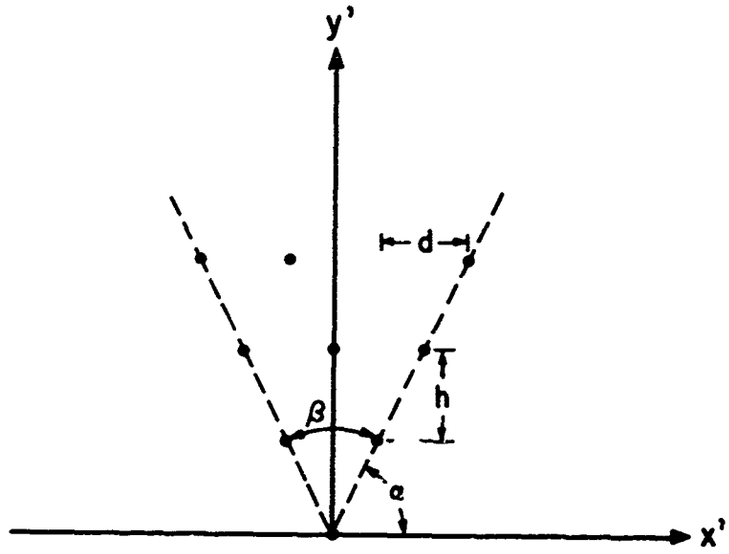

FIG. 2: ISOSCELES TRIANGULAR LATTICE ARRAY

and

$$\vec{r}_{mn}=m\vec{a}_1+n\vec{a}_2=\left\{ma\cos\alpha+na\cos(\alpha+\beta)\right\}\hat{x}' + \left\{ma\sin\alpha+na\sin(\alpha+\beta)\right\}\hat{y}' \quad . \tag{8}$$

Let the distance of separation between two adjacent elements in a row be d, and the distance of separation between two adjacent rows of elements be h. It follows that

$$\bar{r}_{mn}=(m-n)\left(\frac{d}{2}\right)\hat{x}' + (m+n)(h)\,\hat{y}' \quad , \tag{9}$$

and

$$r_{mn}=\left[(m-n)^2\left(\frac{d}{2}\right)^2+(m+n)^2(h)^2\right]^{1/2} \quad . \tag{10}$$

In addition, if $\delta_1=\delta_2=\delta$, then the phase of the (m,n)'th element becomes

$$\delta_{mn}=(m+n)\delta \quad . \tag{11}$$

The fact that m+n is a constant for the elements in the same row makes the array progressively phased between adjacent rows.

In this report we consider only the case where the dipole moments are parallel to the x'-axis. The resultant field in (6) then becomes

$$\vec{E}=A\,\frac{e^{-jkR}}{R}\sin\theta_p\,\hat{\theta}_p\sum_{m=o}^{N-1}\sum_{n=o}^{N-m-1}e^{j(m+n)\delta}\,e^{jkr_{mn}\cos(\phi-\phi_{mn})\sin\theta} \quad , \tag{12}$$

where θ_p is the angle between $\vec{p}$ and $\vec{R}$.

In each of the complex phase factors, we note that

$$r_{mn}\cos(\phi-\phi_{mn})=r_{mn}\cos\phi_{mn}\cos\phi+r_{mn}\sin\phi_{mn}\sin\phi$$

and from (9) and (10),

$$r_{mn}\cos\phi_{mn}=(m-n)\frac{d}{2}\,, \qquad r_{mn}\sin\phi_{mn}=(m+n)h\,.$$

Hence,

$$e^{j(m+n)\delta}\, e^{jkr_{mn}\cos(\phi-\phi_{mn})\sin\theta}$$

$$= e^{j(m+n)\left\{kh\sin\phi\sin\theta+\delta\right\}}\, e^{j(m-n)k\frac{d}{2}\cos\phi\sin\theta} . \qquad (13)$$

In order to steer the main beam to any particular direction, say (ϕ_o, θ_o), we can set

$$\delta = -kh\sin\phi_o\sin\theta_o$$

and (12) can be rewritten as

$$\vec{E} = A\frac{e^{-jkR}}{R}\sin\theta_p\,\hat{\theta}_p \sum_{m=o}^{N-1}\sum_{n=o}^{N-m-1} e^{j(m+n)kh\left\{\sin\phi\sin\theta-\sin\phi_o\sin\theta_o\right\}}$$

$$\times\, e^{j\frac{(m-n)}{2}kd\cos\phi\sin\theta} . \qquad (14)$$

The radiation intensity or the power per unit solid angle is obtained as follows:

$$U(\theta,\phi) = \frac{R^2}{2\eta_o}\vec{E}\cdot\vec{E}^{*} = \frac{A^2}{2\eta_o}\sin^2\theta_p \sum_{m=o}^{N-1}\sum_{n=o}^{N-m-1}\sum_{m'=o}^{N-1}\sum_{n'=o}^{N-m-1}$$

$$\times\, e^{-j\left[(m-m')+(n-n')\delta\right]} e^{jk\left[r_{mn}\cos(\phi-\phi_{mn})-r_{m'n'}\cos(\phi-\phi_{m'n'})\right]\sin\theta} . \qquad (15)$$

the asterisk denotes the complex conjugate of the quantity.

It is noted that the factor involving the multiple summations is proportional to the radiation intensity of the isotropic sources of the like configurations.

III

THE MAXIMUM NOMINAL DIRECTIVITY

In terms of the radiation intensity function, $U(\theta, \phi)$, the directivity function can be deinfed by the relation

$$D(\theta, \phi) = \frac{U(\theta, \phi)}{U_{av}} \quad , \tag{16}$$

where

$$U_{av} = \frac{1}{4\pi} \int_0^{\pi} \int_0^{2\pi} U(\theta, \phi) \sin\theta d\theta d\phi \quad . \tag{17}$$

When the elements are uniformly excited and progressively phased, we shall speak of the directivity of such an array as the nominal directivity. In the sequel, we shall discuss only the maximum directivity, or

$$D_{max}(\theta, \phi) = \frac{U_{max}}{U_{av}} \quad . \tag{18}$$

Henceforth, we shall call this quantity the maximum nominal directivity or simply the directivity.

From Eq. (15)

$$U(\theta, \phi) \sim \sin^2\theta_p \sum_{m=o}^{N-1} \sum_{n=o}^{N-m-1} \sum_{m'=o}^{N-1} \sum_{n'=o}^{N-m'-1} e^{j\left\{(m-m')+(n-n')\right\}\delta}$$

$$e^{jk\left\{r_{mn}\cos(\phi-\phi_{mn})-r_{m'n'}\cos(\phi-\phi_{m'n'})\right\}\sin\theta}$$

$$= \sin^2\theta_p \sum \sum \sum \sum e^{j\left\{(m-m')+(n-n')\right\}\delta}$$

$$e^{jk\left\{\left[r_{mn}\cos\phi_{mn} - r_{m'n'}\cos\phi_{m'n'}\right]\cos\phi + \left[r_{mn}\sin\phi_{mn} - r_{m'n'}\sin\phi_{m'n'}\right]\sin\phi\right\}\sin\theta} \quad . \tag{19}$$

It is readily seen that

$$(r_{mn}\cos\phi_{mn}-r_{m'n'}\cos\phi_{m'n'})\cos\phi+(r_{mn}\sin\phi_{mn}-r_{m'n'}\sin\phi_{m'n'})\sin\phi$$

$$=\left[(m-n)\frac{d}{2}-(m'-n')\frac{d}{2}\right]\cos\phi+\left[(m+n)h-(m'+n')h\right]\sin\phi$$

$$=\left[(m-m')-(n-n')\right]\frac{d}{2}\cos\phi+\left[(m-m')+(n-n')\right]h\sin\phi\ .$$

Put

$$m-m'=p,\ n-n'=q\ , \tag{20}$$

then

$$r_{mn}\cos(\phi-\phi_{mn})-r_{m'n'}\cos(\phi-\phi_{m'n'})=(p-q)\frac{d}{2}\cos\phi+(p+q)h\sin\phi$$

$$=D_{pq}\cos(\phi-\phi_{pq})\quad , \tag{21}$$

where

$$D_{pq}=\left[(p-q)^2\left(\frac{d}{2}\right)^2+(p+q)^2h^2\right]^{1/2} \tag{22}$$

and

$$\cos\phi_{pq}=\frac{(p-q)(d/2)}{D_{pq}}\ . \tag{23}$$

Hence

$$U(\theta,\phi)\sim\sin^2\theta_p\sum_p\sum_q B_{pq}\,e^{j(p+q)\delta}\,e^{jkD_{pq}\cos(\phi-\phi_{pq})\sin\theta} \tag{24}$$

and

$$U_{av}\sim\frac{1}{4\pi}\int_\Omega U(\theta,\phi)\,d\Omega=\sum_p\sum_q B_{pq}\,\frac{e^{j(p+q)\delta}}{4\pi}$$

$$\int_\Omega\sin^2\theta_p\,e^{jkD_{pq}\cos(\phi-\phi_{pq})\sin\theta}\,d\Omega \tag{25}$$

where p, q run through all the meaningful combinations of m-m', and n-n' respectively. B_{pq} is a constant depending on m, m', n, and n' that result in the same p and q. The detailed discussion of B_{pq} will be taken up in a later section.

Let us use the following notation,

$$P_{pq}(D) = \frac{1}{4\pi} \int_{\Omega} e^{jkD_{pq}\cos(\phi-\phi_{pq})\sin\theta} \sin^2\theta_p \, d\Omega \quad . \tag{26}$$

This is an integral which involves a pair of dipoles.

Before we evaluate this integral, let us consider first the following procedure.

IV

THE INTEGRAL INVOLVING TWO INCLINED DIPOLES

Let $\hat{L}$ be a unit vector along the array axis of a pair of dipoles, and $\hat{P}$ indicates the orientation of each dipole. Now let us construct $\hat{L} \times \hat{P}$ axis which is, of course, perpendicular to both $\hat{P}$ and $\hat{L}$. Let us further construct $\hat{x}$ such that

$$\hat{x} = (\hat{L} \times \hat{P}) \times \hat{L} = \hat{P}(\hat{L} \cdot \hat{L}) - \hat{L}(\hat{P} \cdot \hat{L}) = \hat{P} - \hat{L}\cos\gamma \quad .$$

Thus $\hat{x}$, $\hat{L} \times \hat{P}$, $\hat{L}$ form a set of orthornormal base vectors (see Fig. 3). From Fig. 3, $\hat{P} \cdot \hat{R} = \cos\theta_p$. Since $\hat{P}$ is in the $\hat{x}$ and $\hat{L}$ plane, thus it can be expressed as

$$\hat{P} = \sin\gamma \hat{x} + \cos\gamma \hat{L} \, ,$$

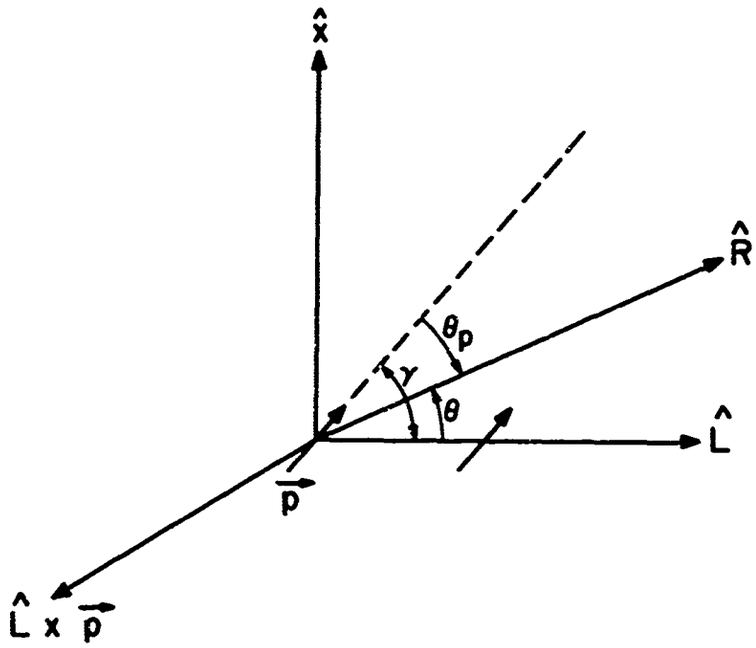

FIG. 3: GEOMETRY OF TWO INCLINED SHORT DIPOLES.

and

$$\hat{R}=\sin\theta\cos\phi\,\hat{x}+\sin\theta\sin\phi(\hat{L}\times\hat{P})+\cos\theta\hat{L}$$

$$\hat{P}\cdot\hat{R}=\sin\gamma\sin\theta\cos\phi+\cos\gamma\cos\theta\ .$$

Therefore

$$\sin^2\theta_p=1-(\hat{R}\cdot\hat{P})^2=1-\left[\cos^2\gamma\cos^2\theta+\frac{1}{2}\sin2\theta\sin2\gamma\cos\phi+\sin^2\gamma\sin^2\theta\cos^2\phi\right]\ .$$

It can be readily shown that the exponent in (26) is transformed to $kD_{pq}\cos\theta$ in the new system of coordinates.

Thus

$$P_{pq}(D)=\frac{1}{4\pi}\int_\Omega \sin^2\theta_p e^{jkD_{pq}\cos\theta}d\Omega$$

$$=\frac{1}{2}\int_0^\pi\left[1-\cos^2\gamma\cos^2\theta-\frac{1}{2}\sin^2\gamma\sin^2\theta\right]e^{jkD_{pq}\cos\theta}\sin\theta d\theta$$

$$=\frac{1}{2}\int_{-1}^{1}\left[1-(\cos^2\gamma)x^2-(\frac{1}{2}\sin^2\gamma)(1-x^2)\right]e^{jkD_{pq}x}\,dx\ ,$$

or

$$P_{pq}(D)=\frac{1}{2}\left\{\left[(1-\cos2\gamma)+\frac{(1+3\cos2\gamma)}{(kD_{pq})^2}\right]\frac{\sin(kD_{pq})}{(kD_{pq})}-(1-3\cos2\gamma)\frac{\cos(kD_{pq})}{(kD_{pq})^2}\right\}\ .$$

The following is a list of some special cases, where $x = kD$.

1. For parallel dipoles, $\gamma = \pi/2$, we have

$$P(x)=(1-\frac{1}{x^2})\frac{\sin x}{x}+\frac{\cos x}{x}\ ,$$

2. For two colinear dipoles, $\gamma=0$,

$$P(x)=2\left\{\frac{\sin x}{x^3}-\frac{\cos x}{x}\right\}\ ,$$

3. $\gamma = 30^{o}$

$$P(x) = \frac{1}{4}\left[\left(1+\frac{5}{x^2}\right)\frac{\sin x}{x} - \frac{\cos x}{x}\right]$$

4. $\gamma = 60^{o}$

$$P(x) = \frac{1}{4}\left[\left(3-\frac{1}{x^2}\right)\frac{\sin x}{x} + \frac{\cos x}{x}\right]$$

5. $\theta = 45^{o}$

$$P(x) = \frac{1}{2}\left(1+\frac{1}{x^2}\right)\frac{\sin x}{x} - \frac{\cos x}{x^2}$$

6. For $x = 0$

$$P(0) = \frac{2}{3} \text{ , independent of } \gamma .$$

It is of interest to note that for a pair of isotropic point sources P is simply $\sin x/x$. The method used here in evaluating P_{pq} bypasses the necessity of integrating Eq. (26) using spherical Bessel functions (Papas, 1965).

V

EVALUATION OF THE DIRECTIVITY

From Eq. (24) it is seen that

$$U_{max} \sim \left[\frac{1}{2} N(N+1)\right]^2 .$$

Thus the directivity of the triangular array can be written as

$$D = \frac{\left[\frac{1}{2} N(N+1)\right]^2}{\sum_{p}\sum_{q} B_{pq} e^{j(p+q)\delta} P_{pq}(D)} .$$

In order to evaluate the double sum in the expression of the directivity of the array, we find it convenient to construct the following matrices.

1. From eq. (20), we see that p, q vary from-(N-1) to (N - 1). However, not all the combinations of p and q are present because of the triangular arrangement. For those combinations that are present, there are often more than one term with the like (p, q) pair. The following is the (p, q) matrix of 10 elements with N = 4 which is the number of elements along $\vec{a}_1$ or $\vec{a}_2$ axis. The entries in the matrix represent the total number of the pairs of elements with the same p, q indices. They are determined by the following formula,

$$B_{pq} = \frac{1}{2} (N - |\epsilon|) (N - |\epsilon| + 1),$$

where $|\epsilon|$ is determined as follows:

a. If p, q are of like sign, then set $|\epsilon| = |p+q|$, 0 is considered either positive or negative.

b. If p, q are of unlike sign, set $|\epsilon|$ equal to the larger of the two magnitudes.

c. If B_{pq} is non positive, then set it to zero.

p \ q	-3	-2	-1	0	1	2	3
-3				1	1	1	1
-2			1	3	3	3	1
-1		1	3	6	6	3	1
0	1	3	6	10	6	3	1
1	1	3	6	6	3	1	
2	1	3	3	3	1		
3	1	1	1	1			

2. Equally of importance in the directivity calculation is the determination of the distances between pairs of dipoles. Again use is made of the (ρ, q) matrix. Superimposed on the matrix we construct two axes using the two diagonals of the matrix. The principle diagonal is labelled as h-axis representing the distance of separation between rows of dipole elements, and the other as $d/2$ - axis, half the distance between adjacent dipole elements. They are scaled as shown in the matrix. The entries in this matrix represent the multiples of h and $d/2$ that are needed to compute D_{pq}'s (eq. (22)). For clarity we omit from it the (0, 0) element and a few others along the diagonals.

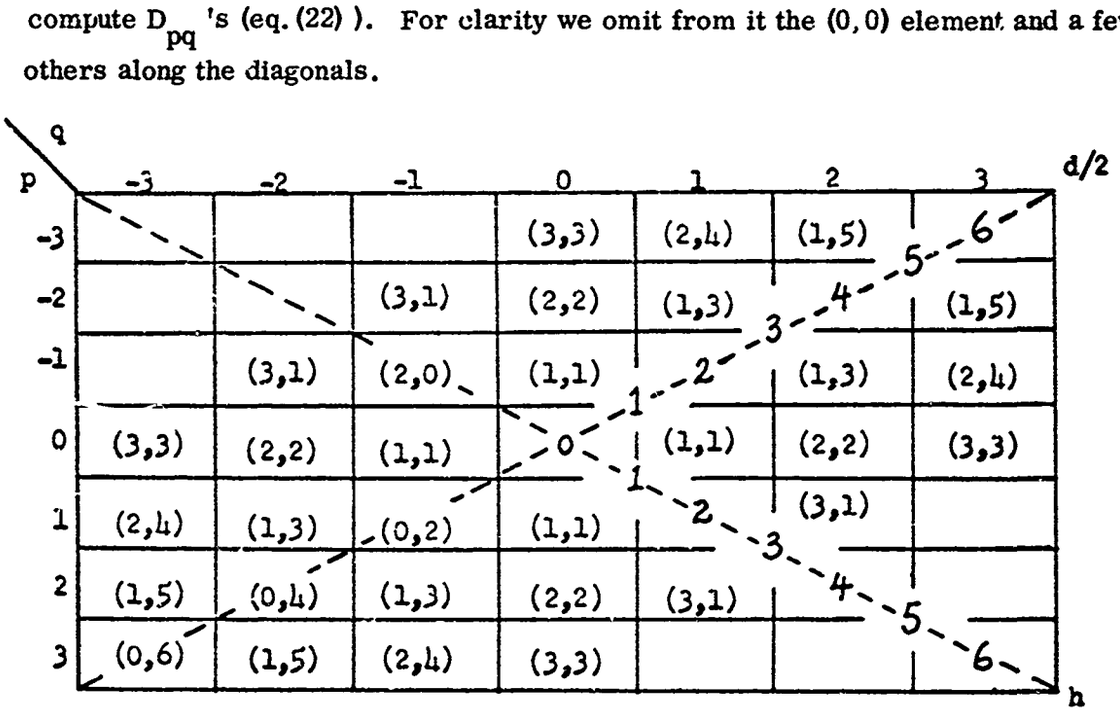

In the expression for $P_{pq}(D)$, the term $\cos 2\gamma$ can be shown to depend on the distances of separations of a pair of dipole elements. In fact, the following relation holds,

$$\cos 2\gamma = \frac{(b\frac{d}{2})^2 - (ah)^2}{(b\frac{d}{2})^2 + (ah)^2}$$

where (a, b) is the ordered pair in the entry in the above matrix.

3. To complete the picture, the (p, q) matrix us used again to indicate the phase relations, which are simply the algebraic sum of p and q times δ. The double sum becomes

$$\sum_{p=-3}^{3} \sum_{q=-3}^{3} e^{j(p+q)} \frac{1}{2} (N-|\epsilon|)(N-|\epsilon|+1) P_{pq}$$

$$= \frac{1}{2} N(N+1) P_{00} + \sum_{p}' \sum_{q}' e^{j(p+q)\delta} \frac{1}{2}(N-|\epsilon|)(N-|\epsilon|+1) P_{pq}$$

$$= \frac{1}{2} N(N+1) \frac{2}{3} + \sum_{p}' \sum_{q}' e^{j(p+q)\delta} \frac{1}{2} (N-|\epsilon|)(N-|\epsilon|+1) P_{pq}$$

where the prime indicates all the p, q combinations with the exception of (0, 0).

VI

NUMERICAL RESULTS

Numerical results of the radiation patterns and directivities of the triangular lattice array are presented here for both the isotropic and the short dipole cases. They are done for the case where the main beam is directed at $\theta=90^{o}$ and $\phi=90^{o}$.

Both the E- and H-planes are included in the computation, however, the discussion will be made only in connection with the E-plane pattern. Tables 1 through 3 sun marize the numerical results as shown in Figs. 4 through 9, with varying paramdeters d (element spacing), h (row spacing) and N (total number of elements in the array).

It is seen from Table 1 for the isotropic case that the beam angle decreases as the spacing between elements increases. At d=0.2λ, the beam angle decreases significantly as the spacing between rows of elements increases. Nevertheless, no discernible changes are observed as h changes at other d's. As compared with the isotropic case, little difference is noticed in the beam angles in the dipole case (Table 2). We are thus led to believe this is purely a characteristic of the triangular lattice arrangement. It is also observed as expected that the beam angle becomes smaller as the number of elements increases.

The radiation patterns for both the isotropic and the dipole cases are symmetric with respect to the x-axis at h = 0 and 0.5λ. This is so because of the progressive phasing selected for the successive rows of elements. For the row spacing between 0 and 0.5λ, the patterns are more directed toward one side. The back lobe levels, which are relative the most prominent among the minor lobes, are identical for both cases considered (Table 3). It also shows that they are smaller at h = 0.2 and 0.3λ at all element spacings.

The side lobes in the isotropic case begin to emerge at $\phi=0^{o}$ at smaller row spacings when the element spacings are small, and at relatively larger row spacing when the element spacings are large. However, the use of dipoles as a radiation source completely eliminates this undesirable effect, and also puts a severe limit on the other side lobes as to render them almost negligible.

Also shown in the tables are the effects of the increasing sizes on the beam angles and the back lobe levels. The larger the size of the array, the smaller the beam angle and the back lobe levels.

The directivity for both the isotropic and the dipole cases is improved as the row spacing increases up to a certain point, then it is tapered off for further increase in the row spacings (Figs. 10a-10d). It reaches a maximum in the neighborhood of h=0.4λ for d's between 0.2 and 0.6λ. Further increase in the element spacing shifts the maximum in the decreasing h direction; for instance, it is at about h=0.35λ for d=0.8λ and at h=0.2λ for d-1.0λ in the isotropic case.

TABLE 1: BEAM ANGLES FOR THE ISOTROPIC CASE OF TEN ELEMENTS.

h/λ	d/λ (Degrees)				
	.2	.4	.6	.8	1.0
0	94	44	29	22	17
.1	92	44	28	22	17
.2	86	44	28	22	17
.3	78	44	28	22	17
.4	74	43	28	22	17
.5	68	42	28	22	17

TABLE 2: BEAM ANGLES OF DIPOLE CASE OF 10, 15, 21 ELEMENTS AT $h/\lambda = 0.2, 0.3, 0.4$.

d/λ	N (Degrees)		
	10	15	21
0.4	40	32	27
0.6	28	22	19
0.8	20	17	15

TABLE 3: BACK LOBE LEVELS OF BOTH THE ISOTROPIC AND THE DIPOLE CASES AT $d/\lambda = 0.4, 0.6, 0.8$.

h/λ	N_t		
	10	15	21
0.2	.069098	.030710	.029274
0.3	.069098	.030710	.029274
0.4	.180902	.080401	.054625

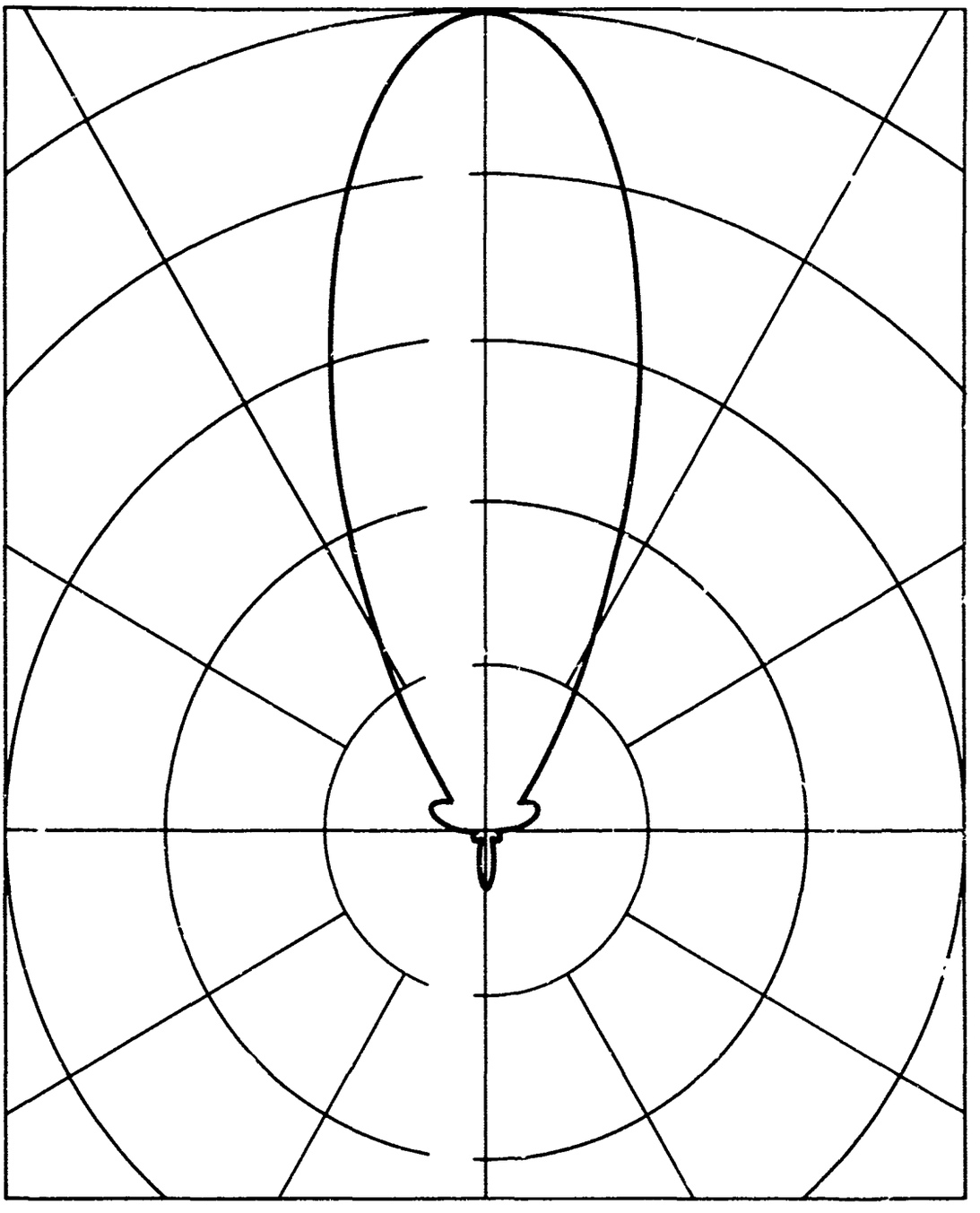

FIG. 4a: The radiation patterns of the triangular lattice arrays with $d/\lambda = 0.4$, $h/\lambda = 0.3$, E-plane pattern of a 10-element isotropic array.

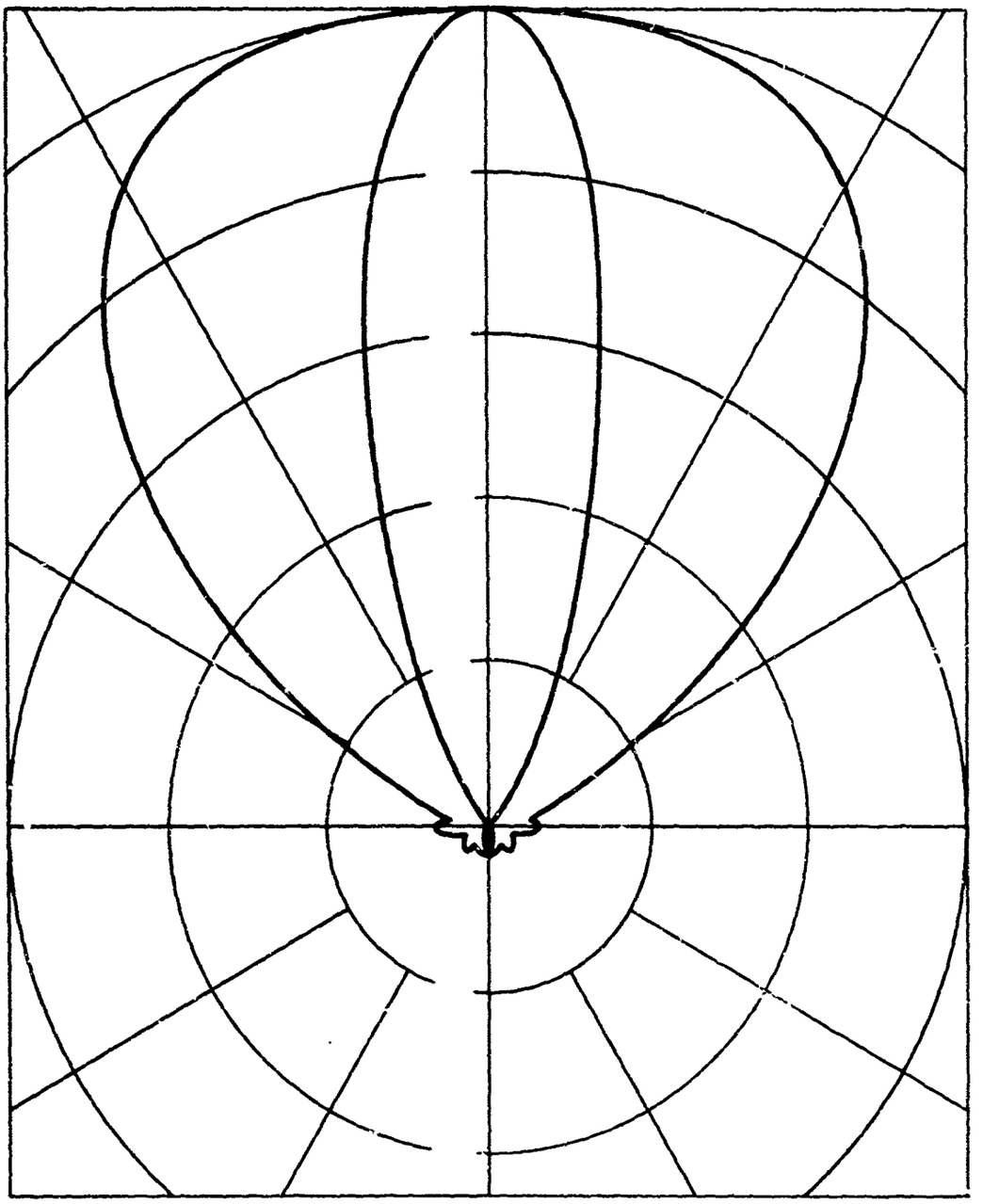

Fig. 4b: The Radiation Patterns of the Triangular Lattice Arrays with $d/\lambda=0.4$, $h/\lambda=0.3$, E- and H-plane Patterns of a 15-element Short Dipole Array.

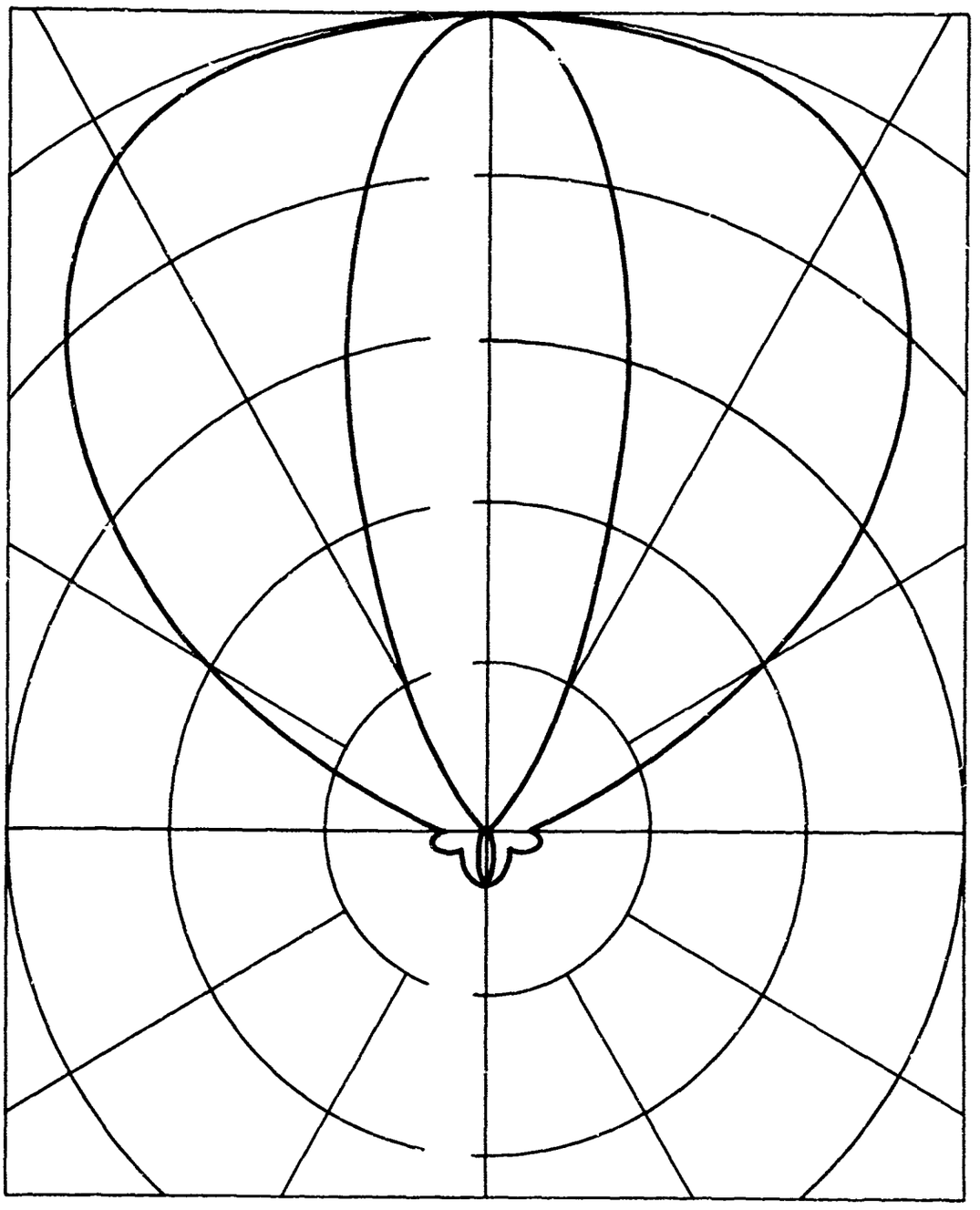

FIG. 4c: The Radiation Pattern of the Triangular Lattice Arrays with $d/\lambda=0.4$, $h/\lambda=0.3$, E-plane (inside curve) and H-plane (outside curve) Patterns of a 10-element Short Dipole Array.

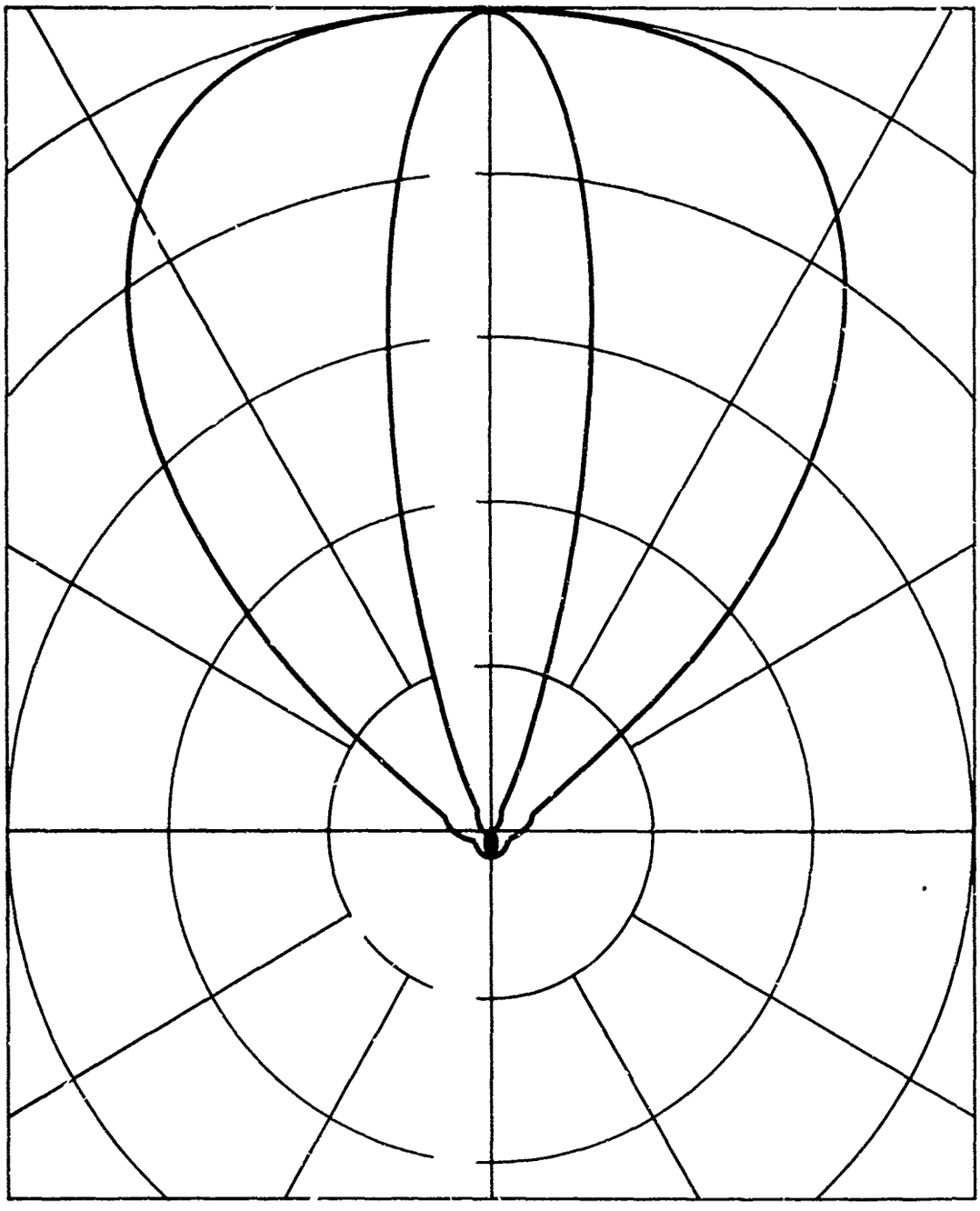

FIG. 4d: The radiation patterns of the triangular lattice arrays with $d/\lambda = 0.4$, $h/\lambda = 0.3$, E- and H-plane patterns of a 21-element short dipole array.

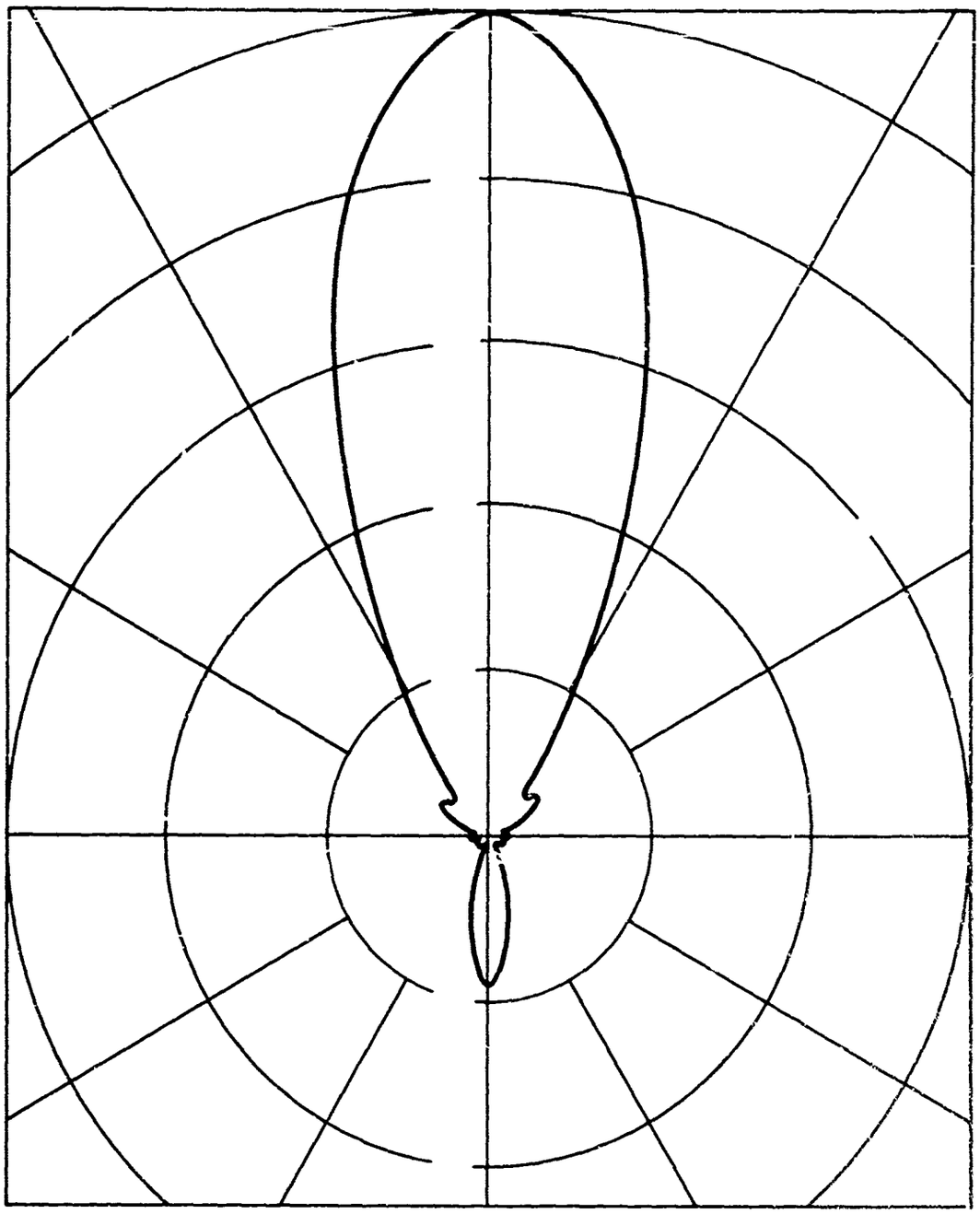

FIG. 5a: The radiation patterns of the triangular lattice array with $d/\lambda = 0.4$, $h/\lambda = 0.4$, E-plane pattern of a 10-element isotropic array.

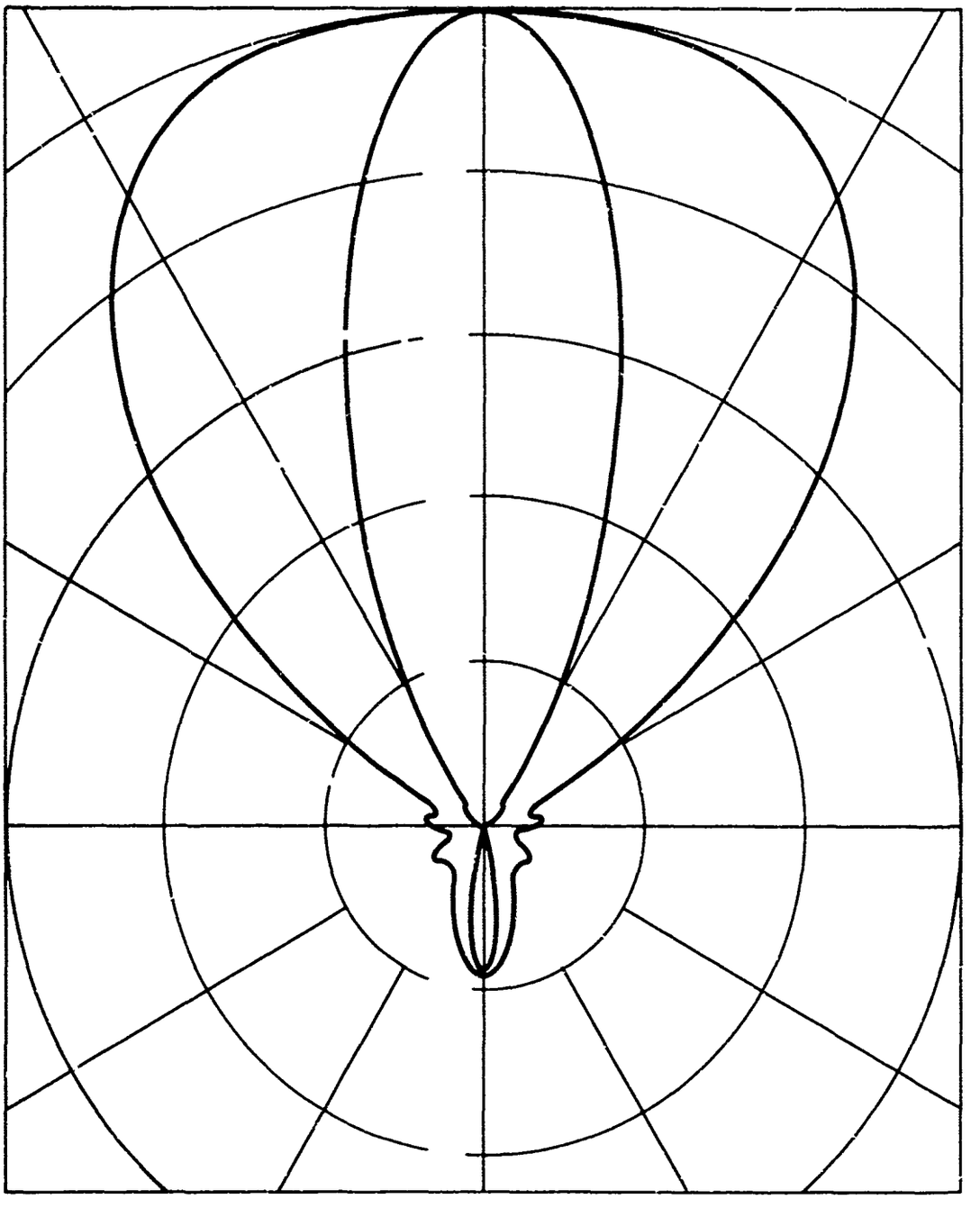

FIG. 5b: The radiation patterns of the triangular lattice array with $d/\lambda = 0.4$, $h/\lambda = 0.4$, E-plane (inside curve) and H-plane (outside curve) patterns of a 10-element short dipole array.

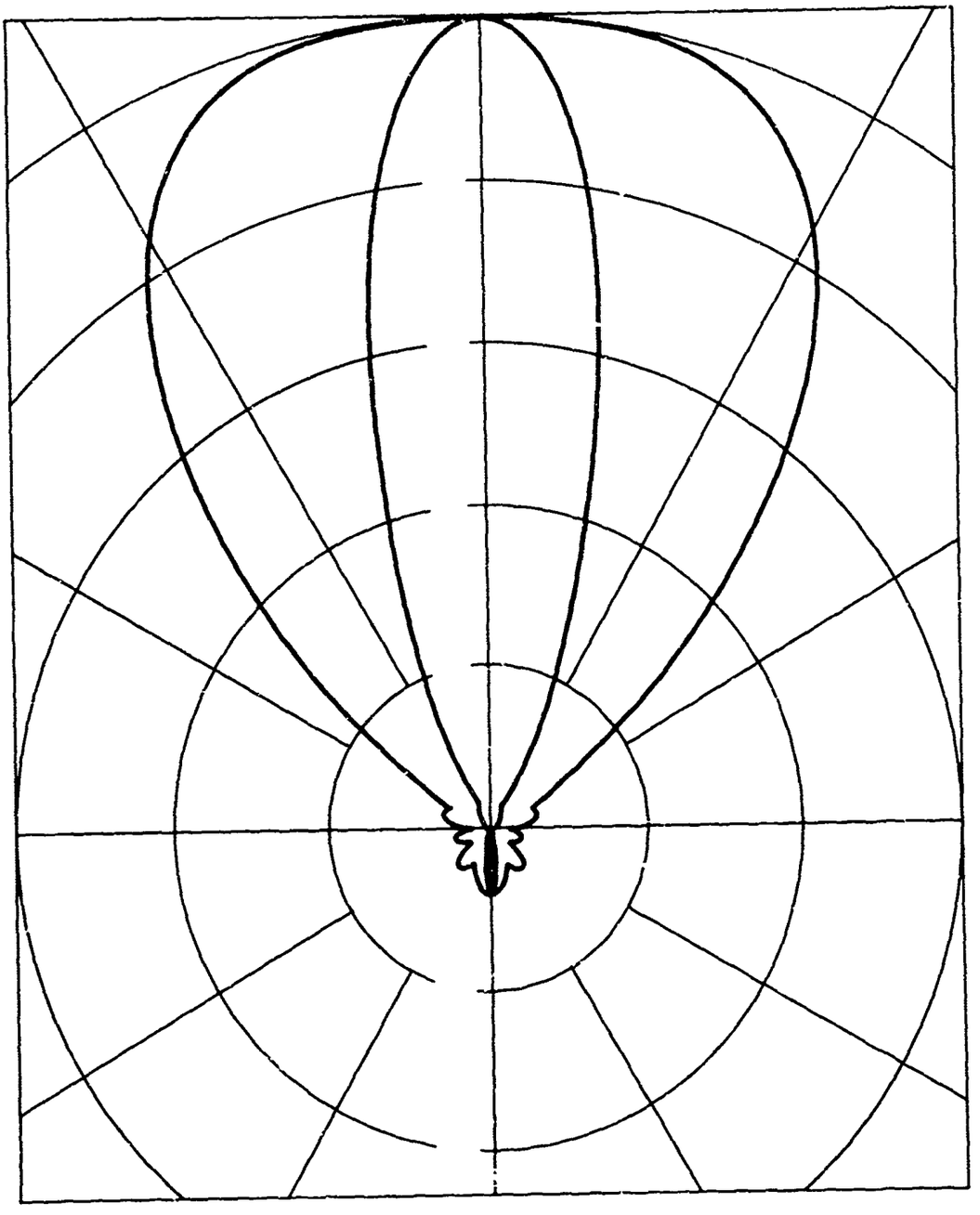

FIG. 5c: The radiation patterns of the triangular lattice array with $d/\lambda = 0.4$, $h/\lambda = 0.4$, E- and H-plane patterns of a 15-element short dipole array.

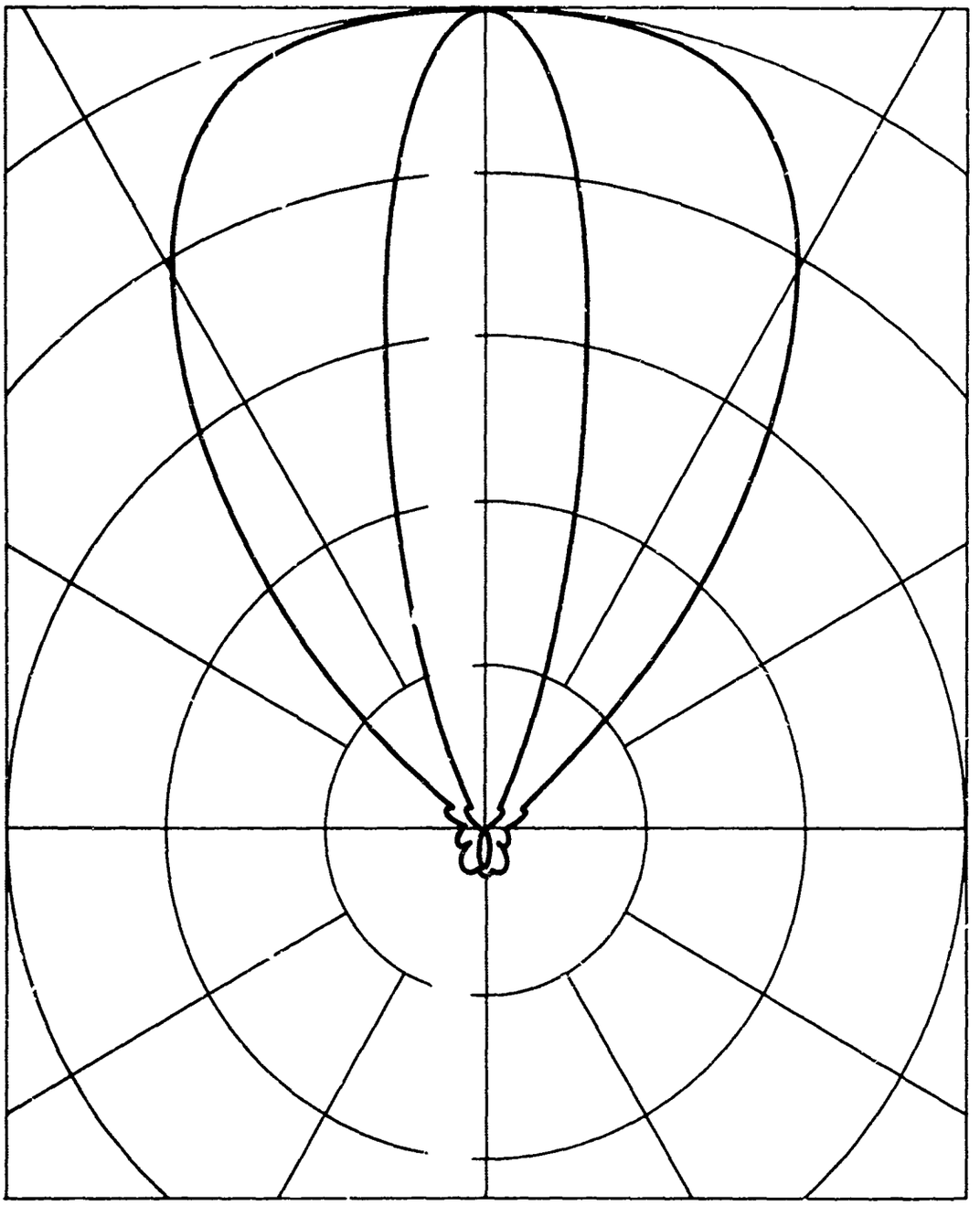

FIG. 5d: The radiation patterns of the triangular lattice array with $d/\lambda = 0.4$, $h/\lambda = 0.4$, E- and H-plane patterns of a 21-element short dipole array.

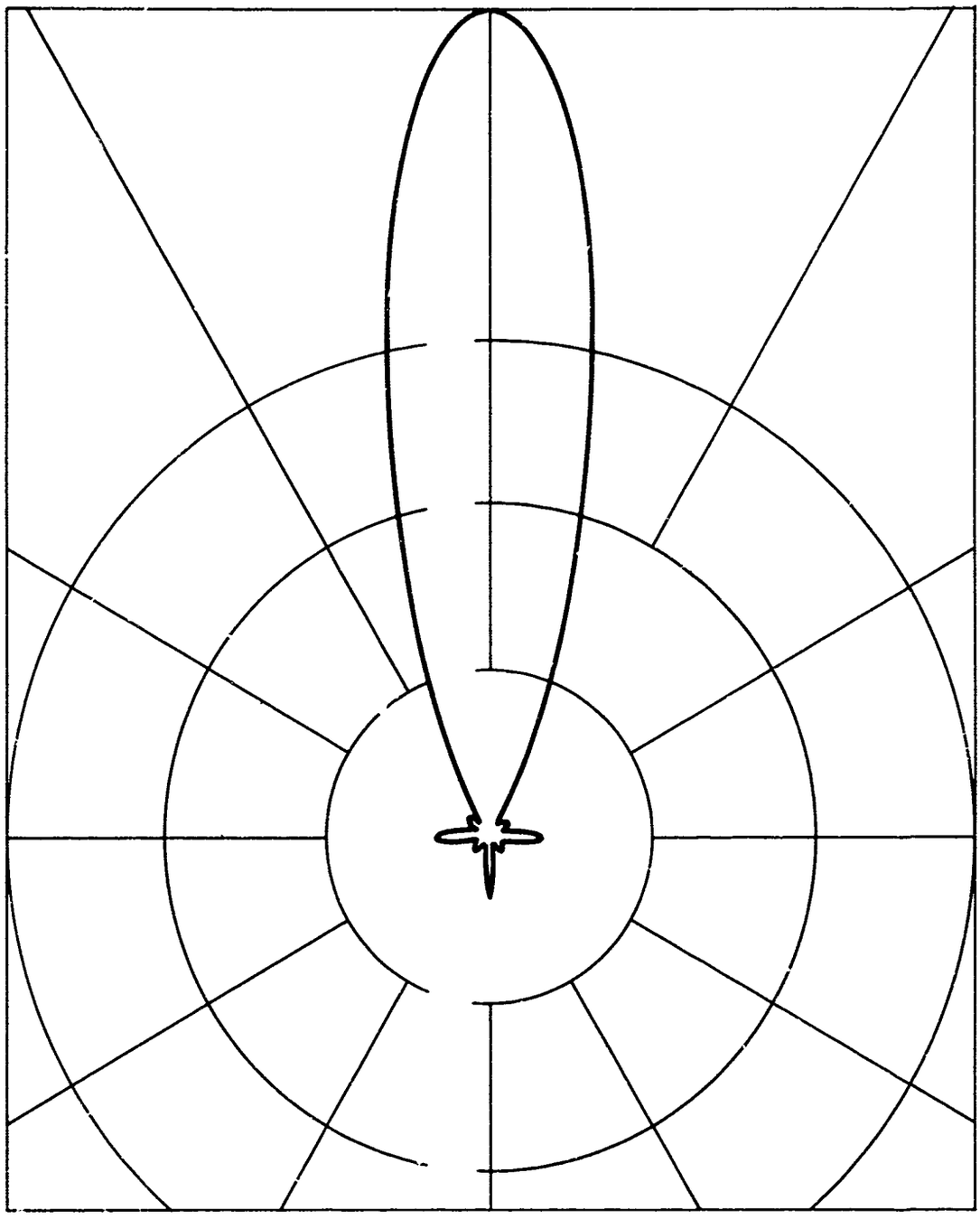

FIG. 6a: The radiation patterns of the triangular lattice arrays with $d/\lambda = 0.6$, $h/\lambda = 0.3$, E-plane pattern of a 10-element isotropic array.

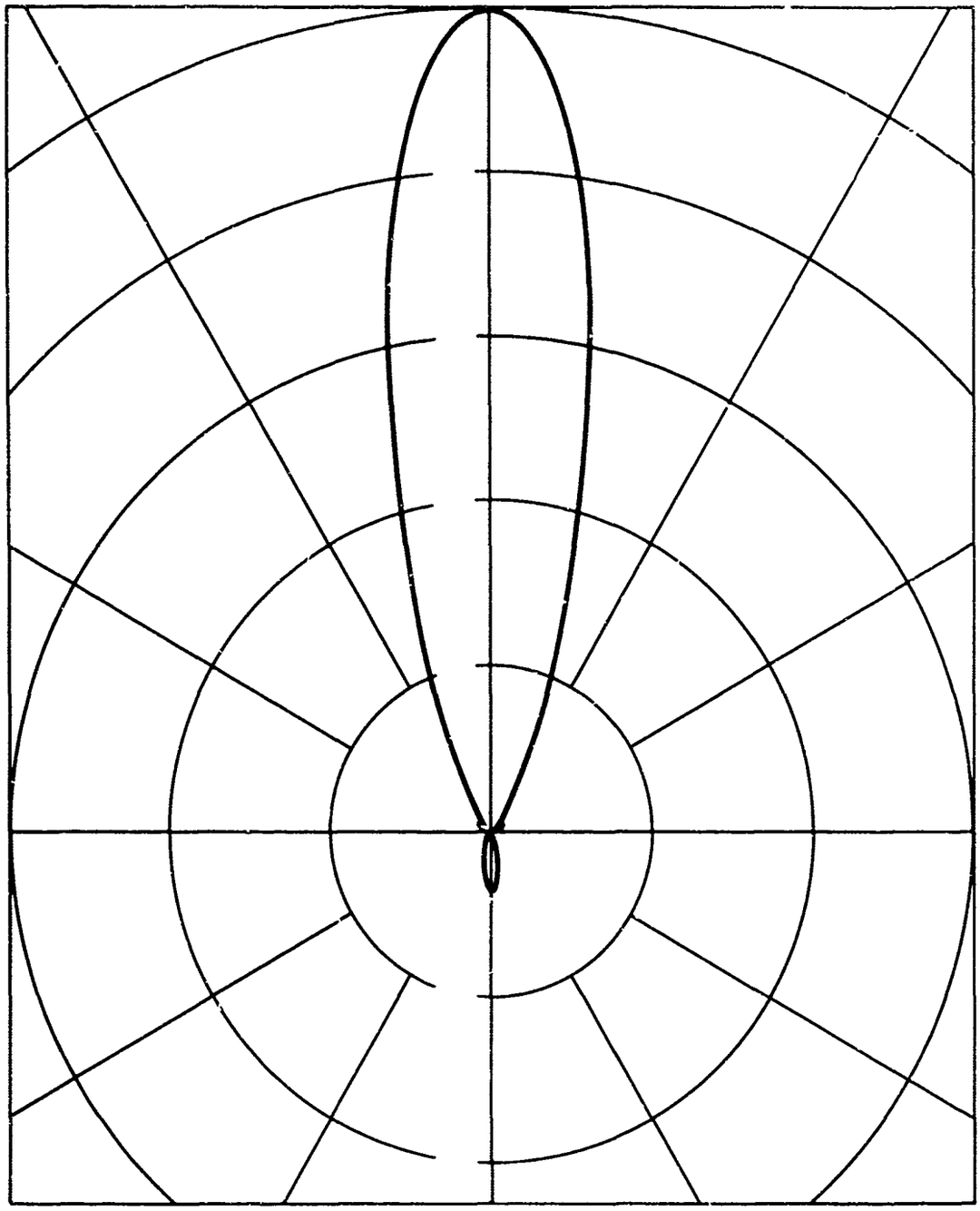

FIG. 6b: The radiation patterns of the triangular lattice arrays with $d/\lambda = 0.6$, $h/\lambda = 0.3$, E-plane pattern of a 10-element short dipole array.

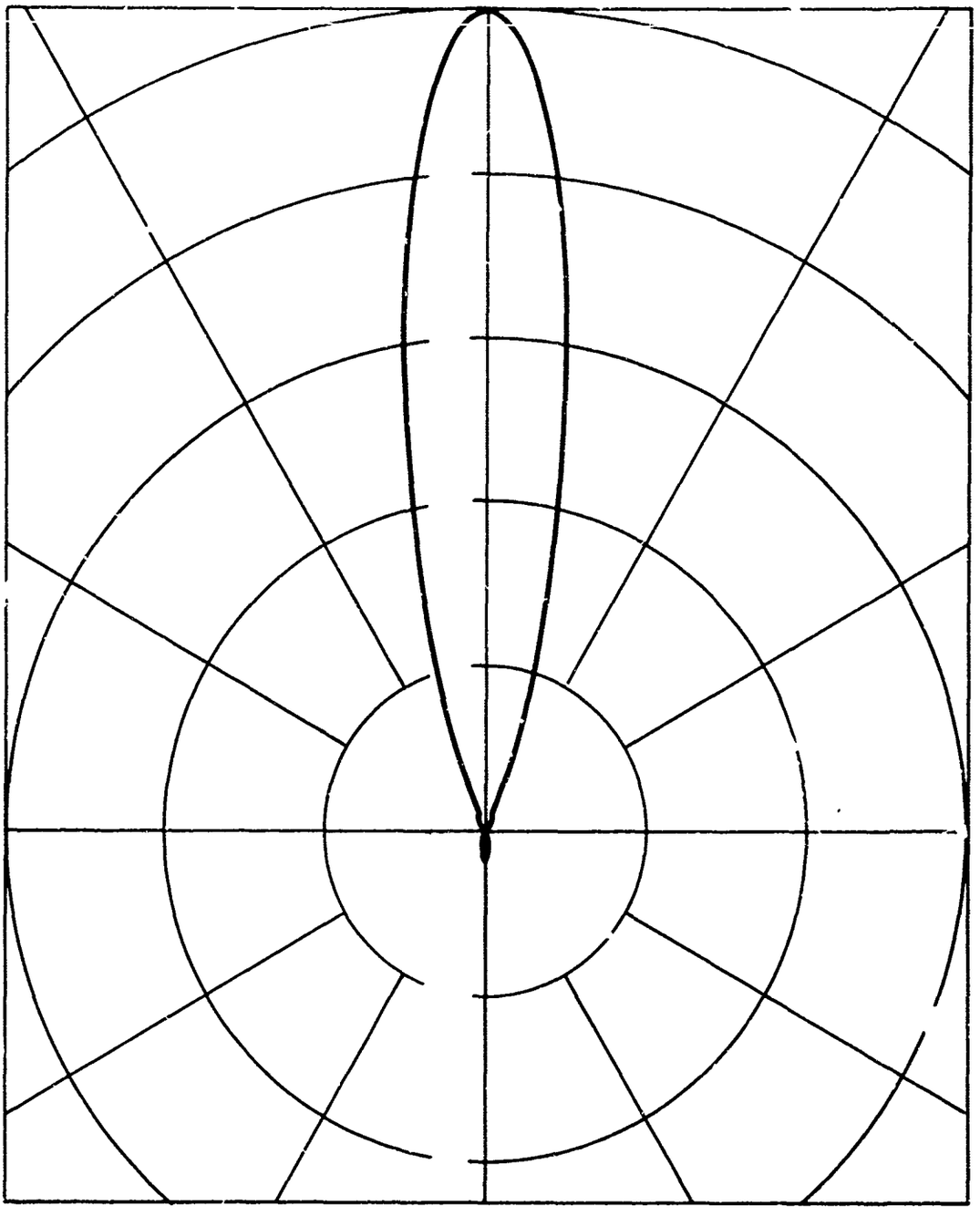

FIG. 6c: The radiation patterns of the triangular lattice arrays with $d/\lambda = 0.6$, $h/\lambda = 0.3$, E-plane pattern of a 15-element short dipole array.

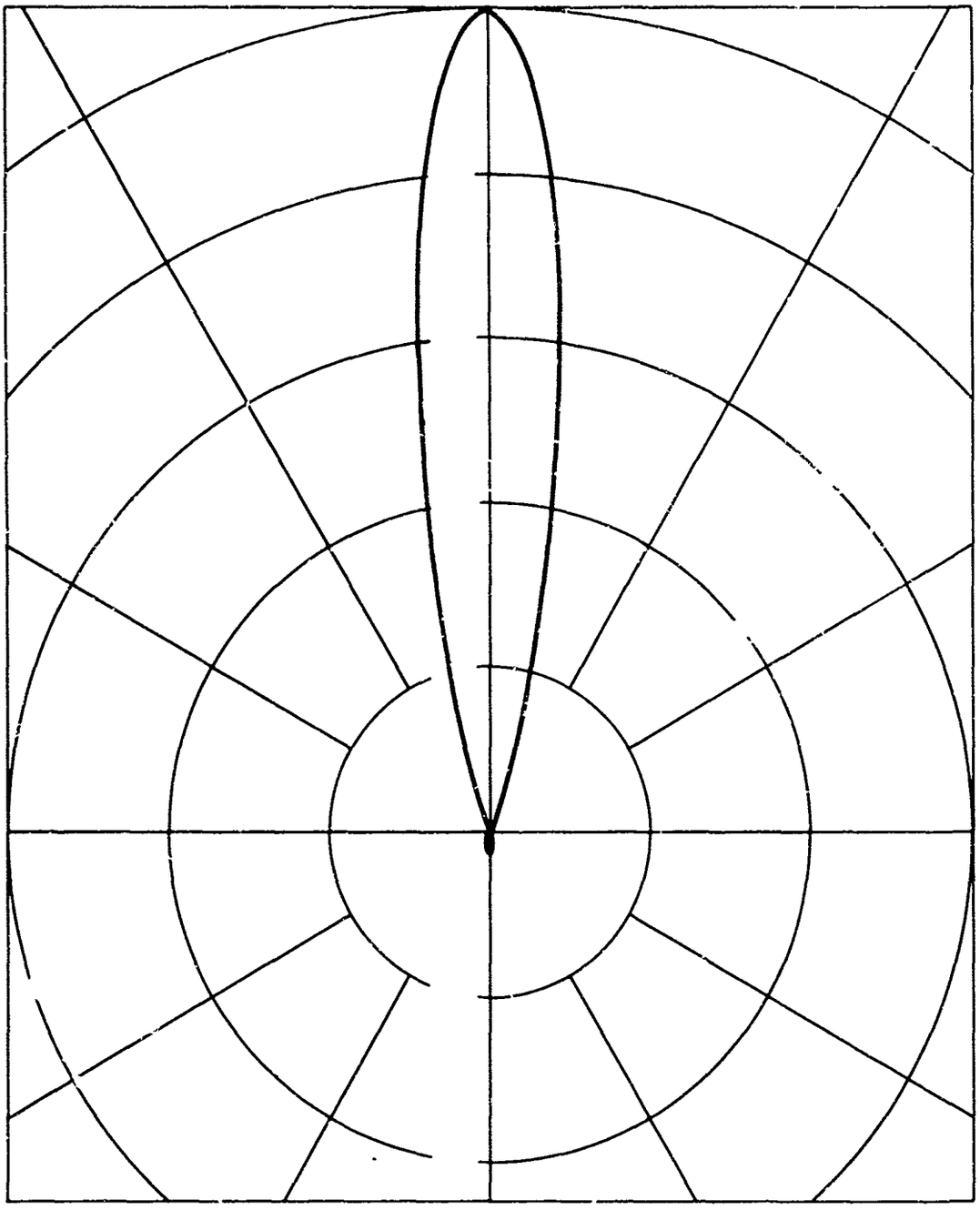

FIG. 6d: The radiation patterns of the triangular lattice arrays with $d/\lambda = 0.6$, $h/\lambda = 0.3$. E-plane pattern of a 21-element short dipole array.

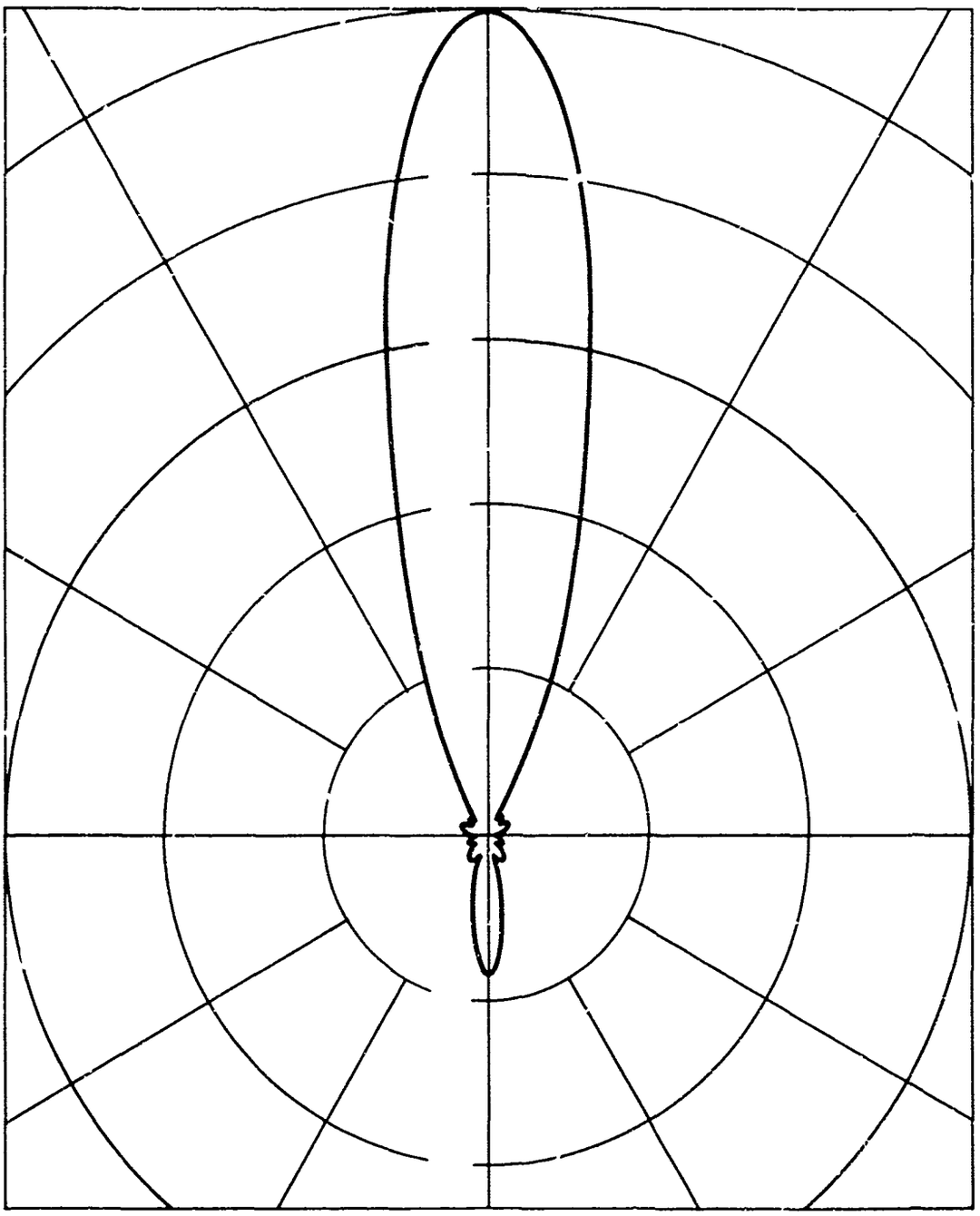

FiG. 7a: The radiation patterns of the triangular lattice arrays with $d/\lambda = 0.6$, $h/\lambda = 0.4$, E-plane pattern of a 10-element isotropic array.

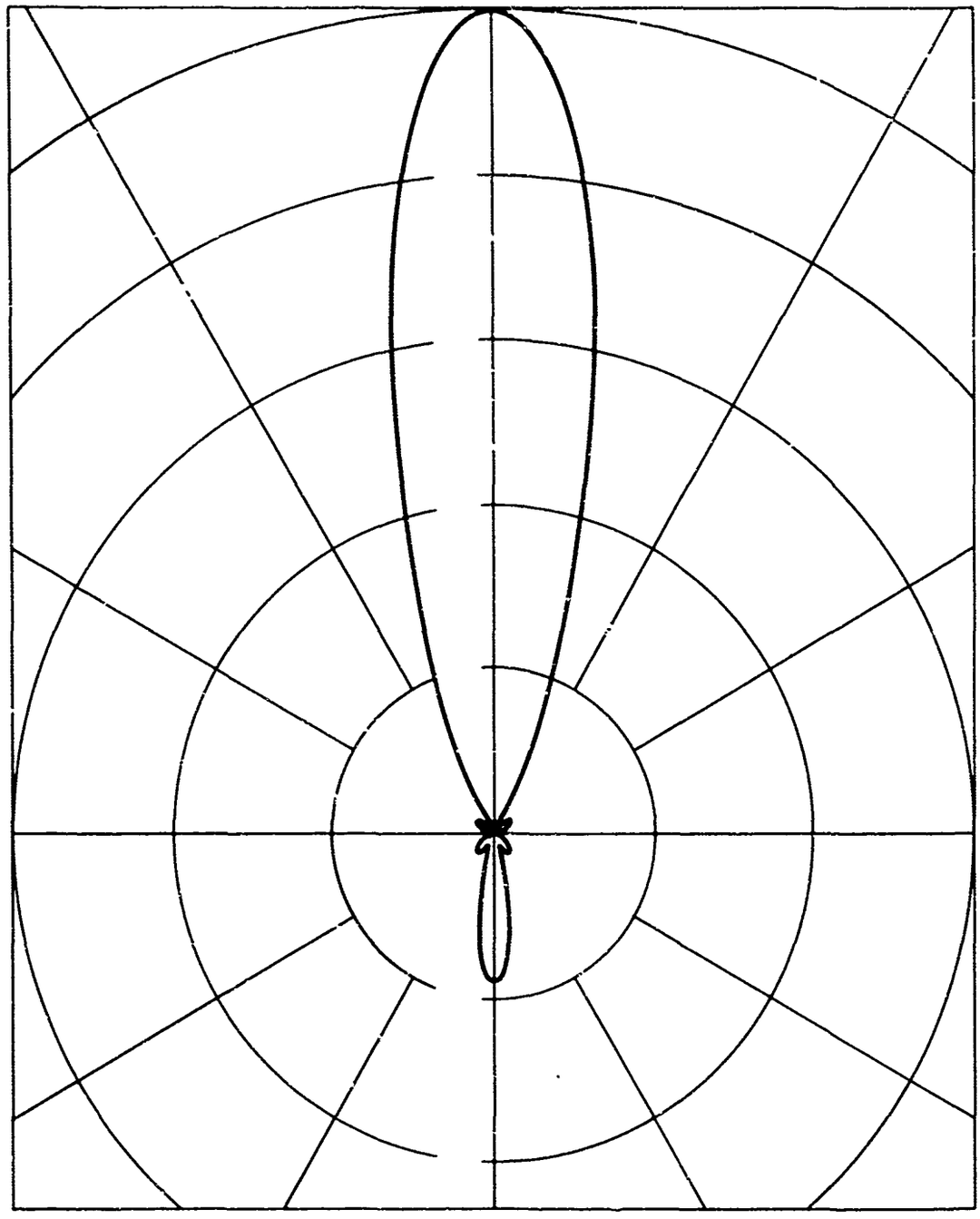

FIG. 7b: The radiation patterns of the triangular lattice arrays with $d/\lambda = 0.6$, $h/\lambda = 0.4$, E-plane pattern of a 10-element short dipole array.

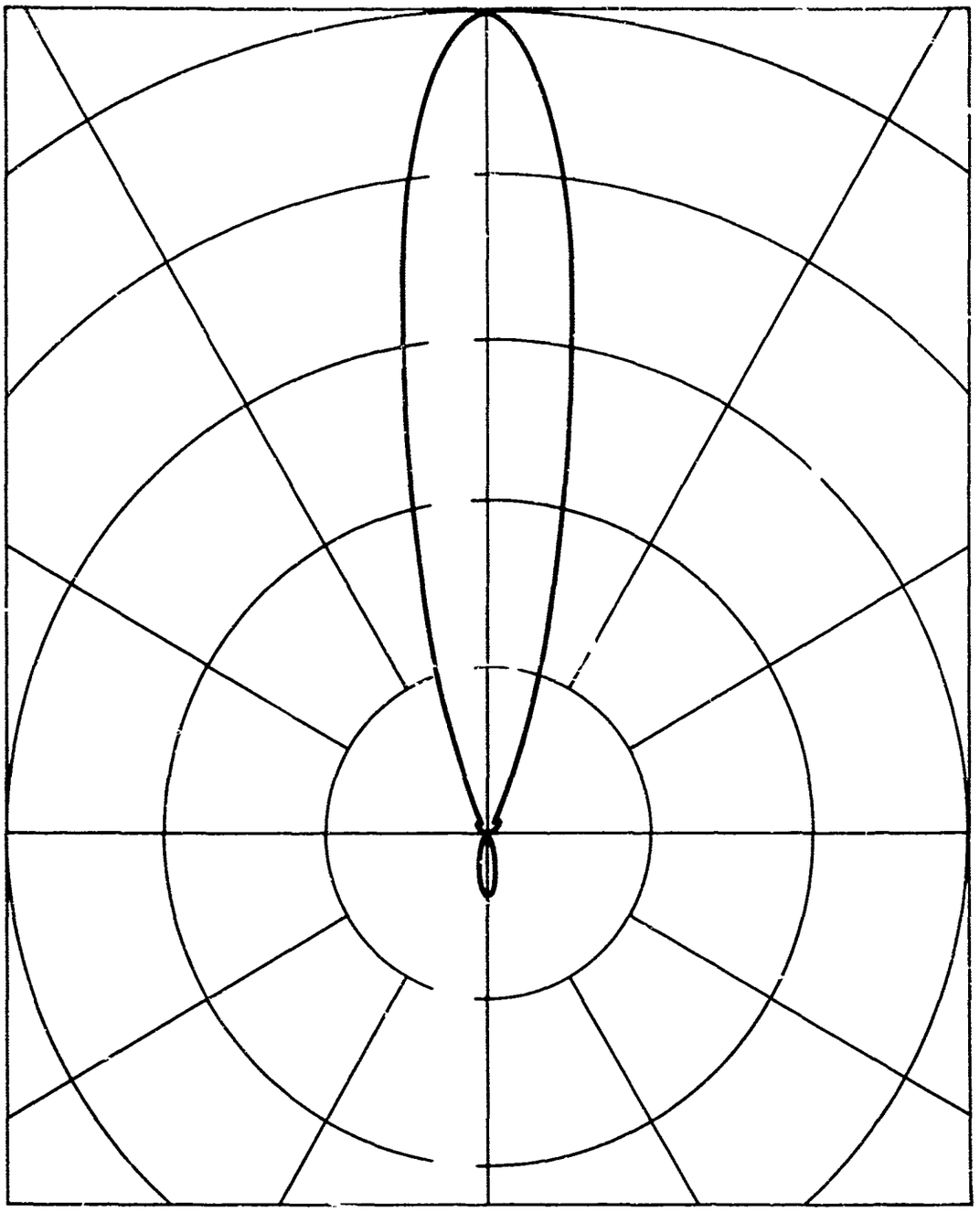

FIG. 7c: The radiation patterns of the triangular lattice arrays with $d/\lambda = 0.6$, $h/\lambda = 0.4$, E-plane pattern of a 15-element short dipole array.

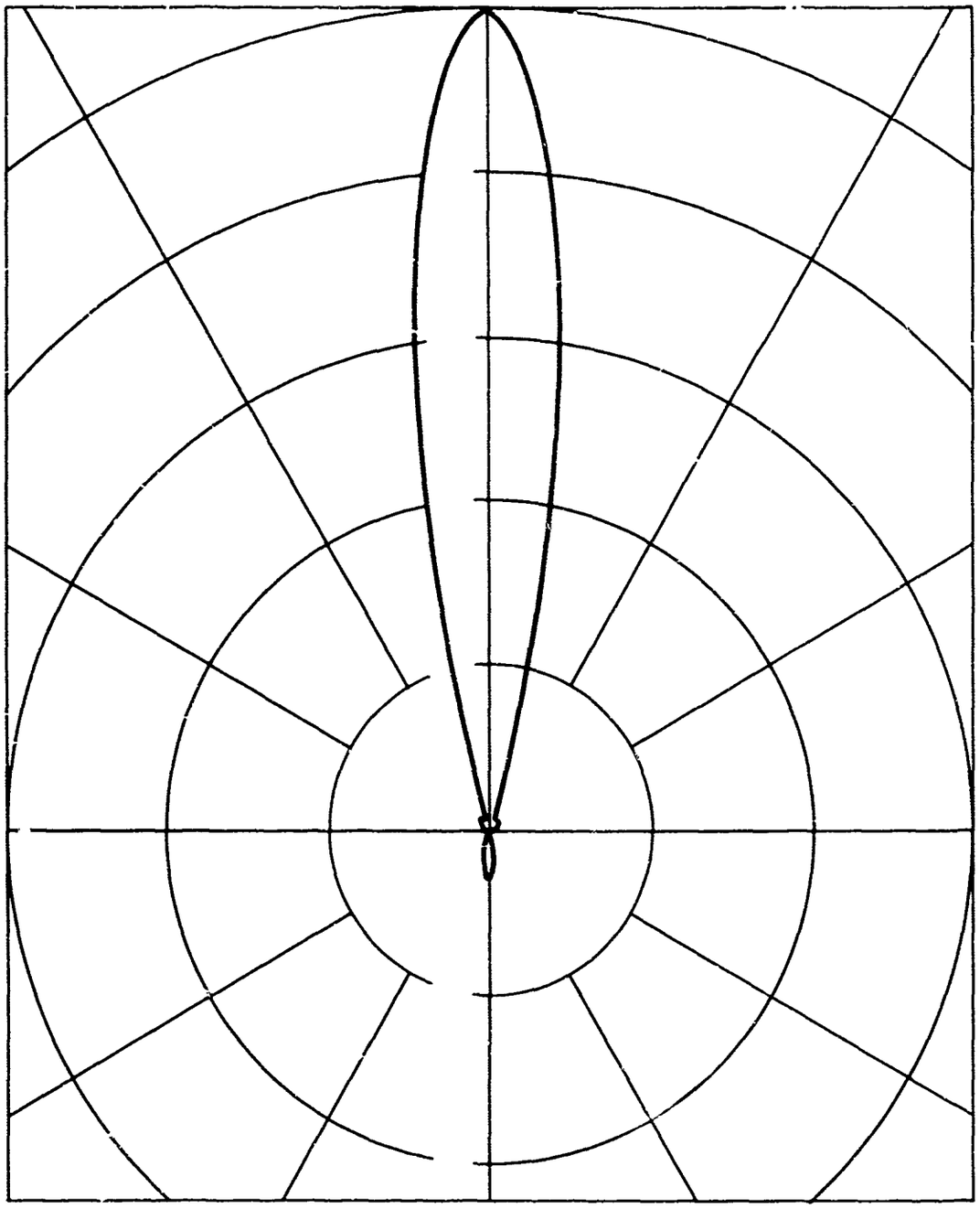

FIG. 7d: The radiation patterns of the triangular lattice arrays with $d/\lambda = 0.6$, $h/\lambda = 0.4$, E-plane pattern of a 21-element short dipole array.

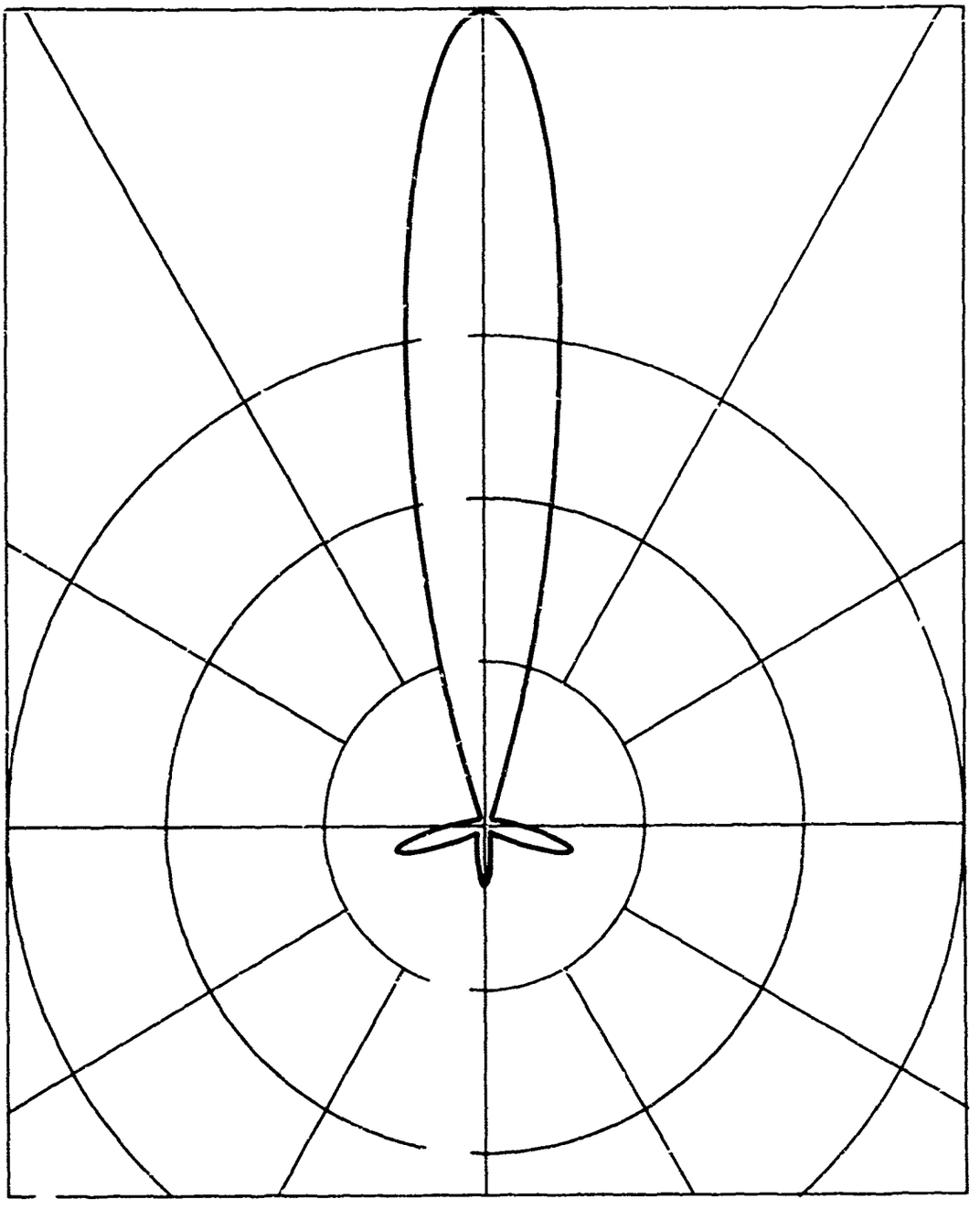

FIG. 8a: The radiation patterns of the triangular lattice arrays with $d/\lambda = 0.8$, $h/\lambda = 0.3$, E-plane pattern of a 10-element isotropic array.

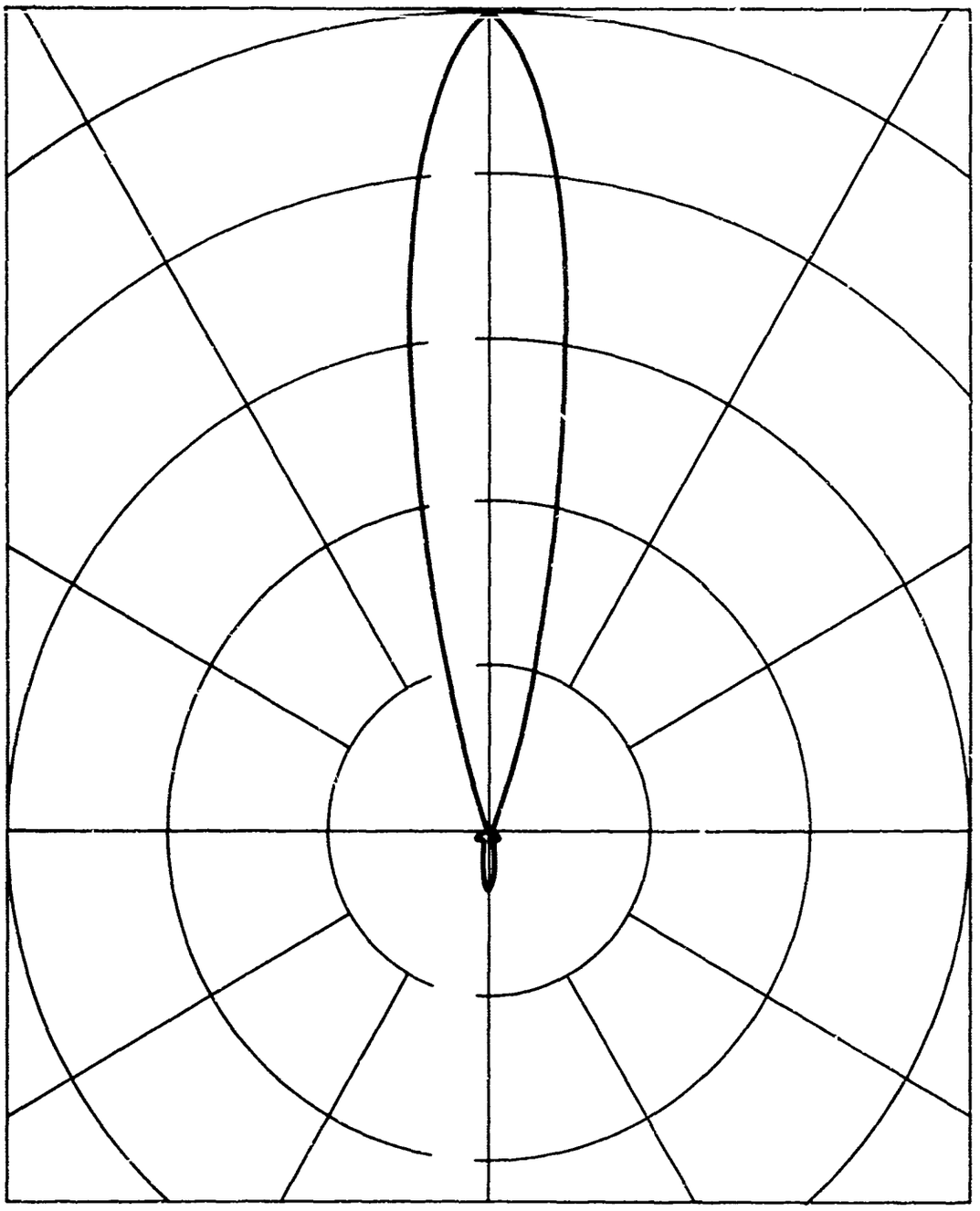

FIG. 8b: The radiation patterns of the triangular lattice arrays with $d/\lambda = 0.8$, $h/\lambda = 0.3$, E-plane pattern of a 10-element short dipole array

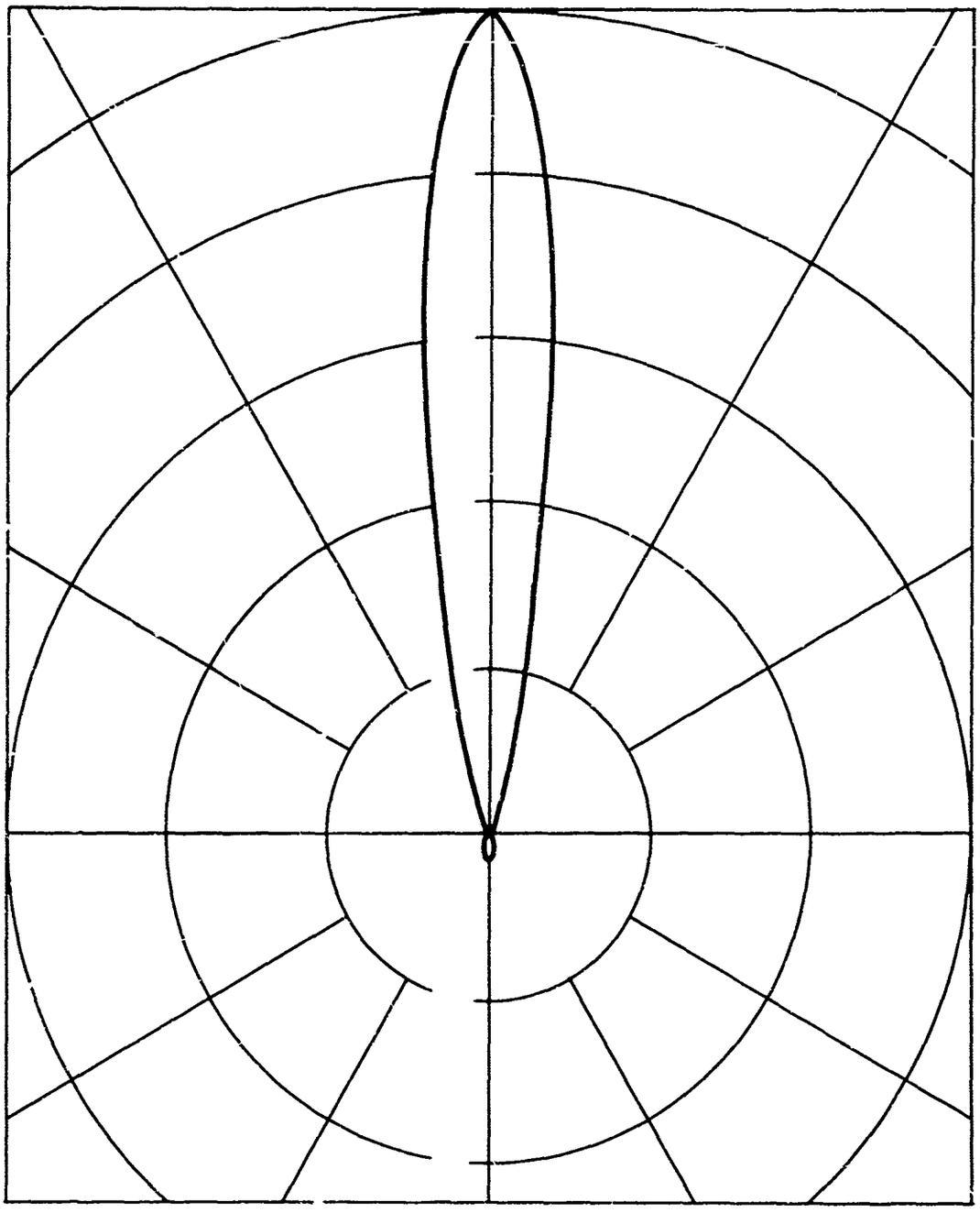

FIG. 8c: The radiation patterns of the triangular lattice arrays with $d/\lambda = 0.8$, $h/\lambda = 0.3$, E-plane pattern of a 15-element short dipole array.

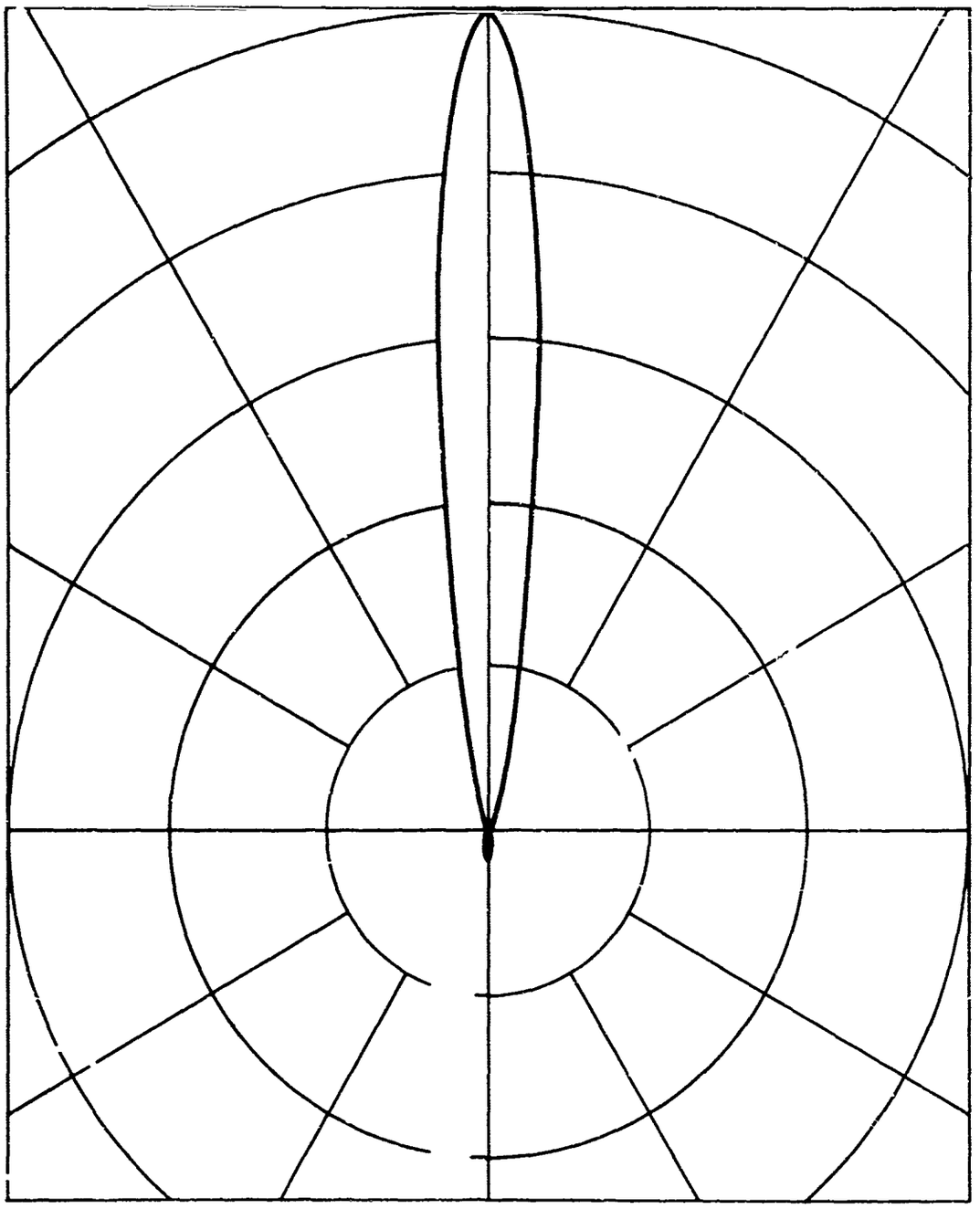

FIG. 8d: The radiation patterns of the triangular lattice arrays with $d/\lambda = 0.8$, $h/\lambda = 0.3$, E-plane pattern of a 21-element short dipole array.

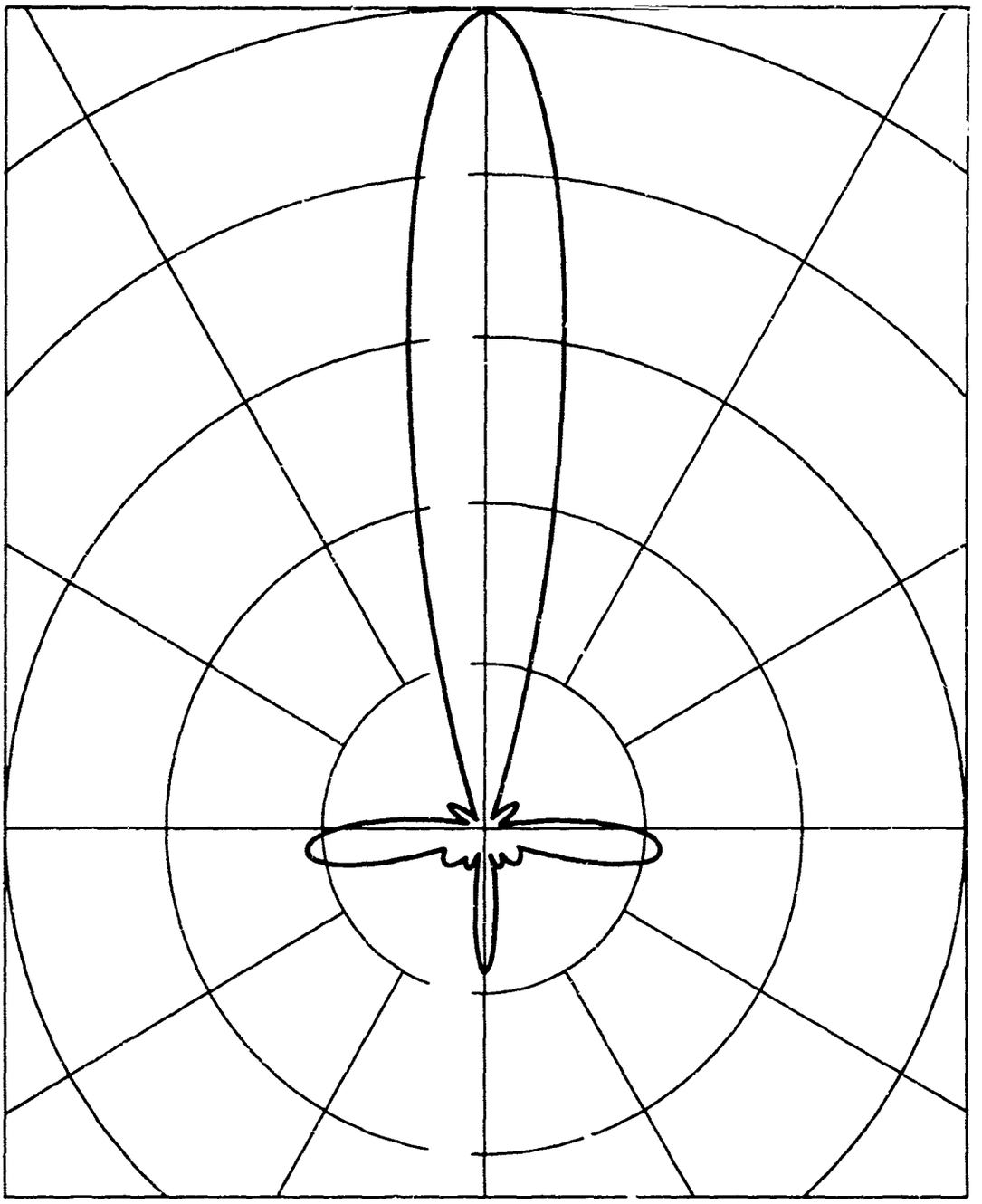

FIG. 9a: The radiation patterns of the triangular lattice arrays with $d/\lambda = 0.8$, $h/\lambda = 0.4$, E-plane pattern of a 10-element isotropic array.

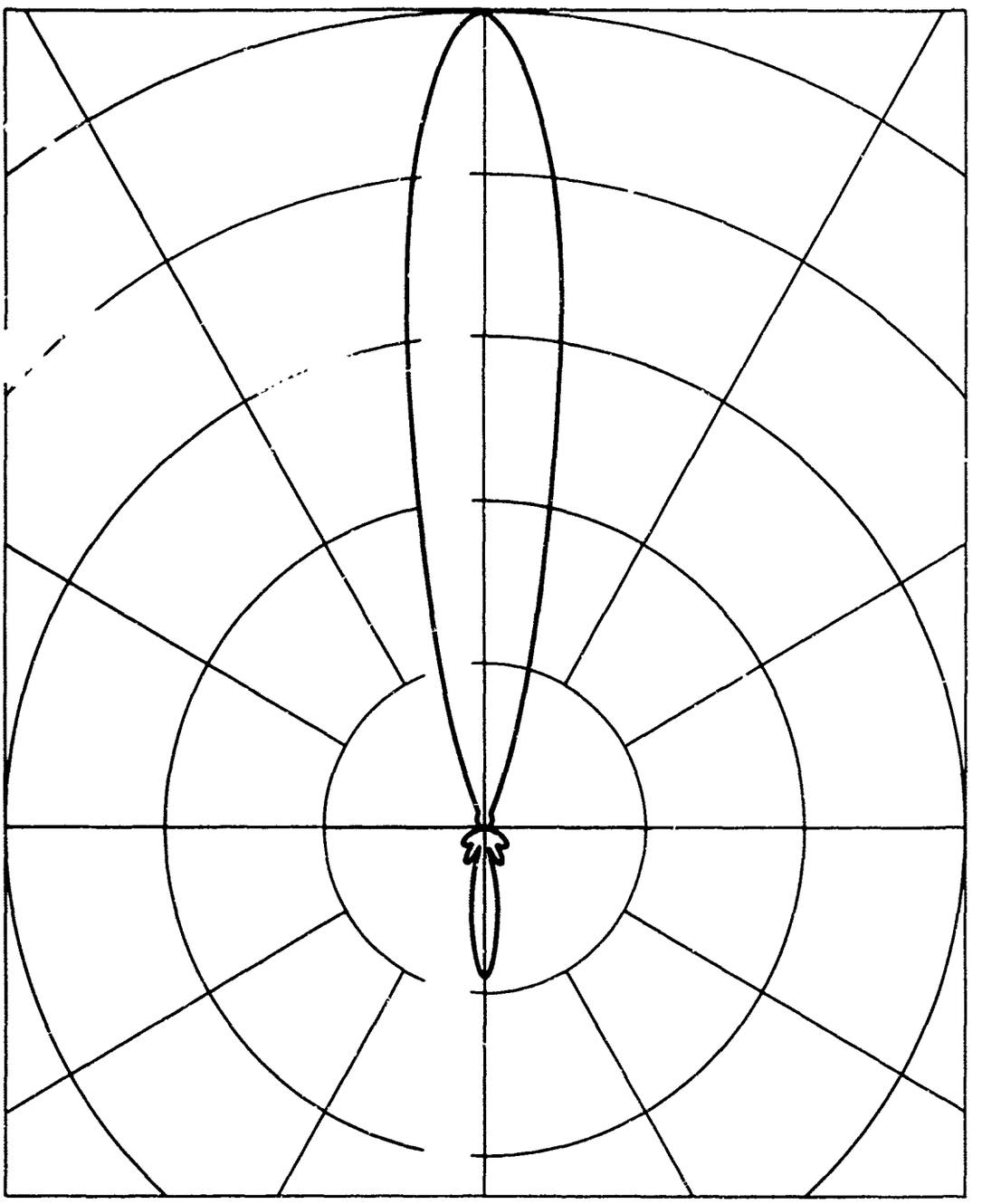

FIG. 9b: The radiation patterns of the triangular lattice arrays with $d/\lambda = 0.8$, $h/\lambda = 0.4$, E-plane pattern of a 10-element short dipole array.

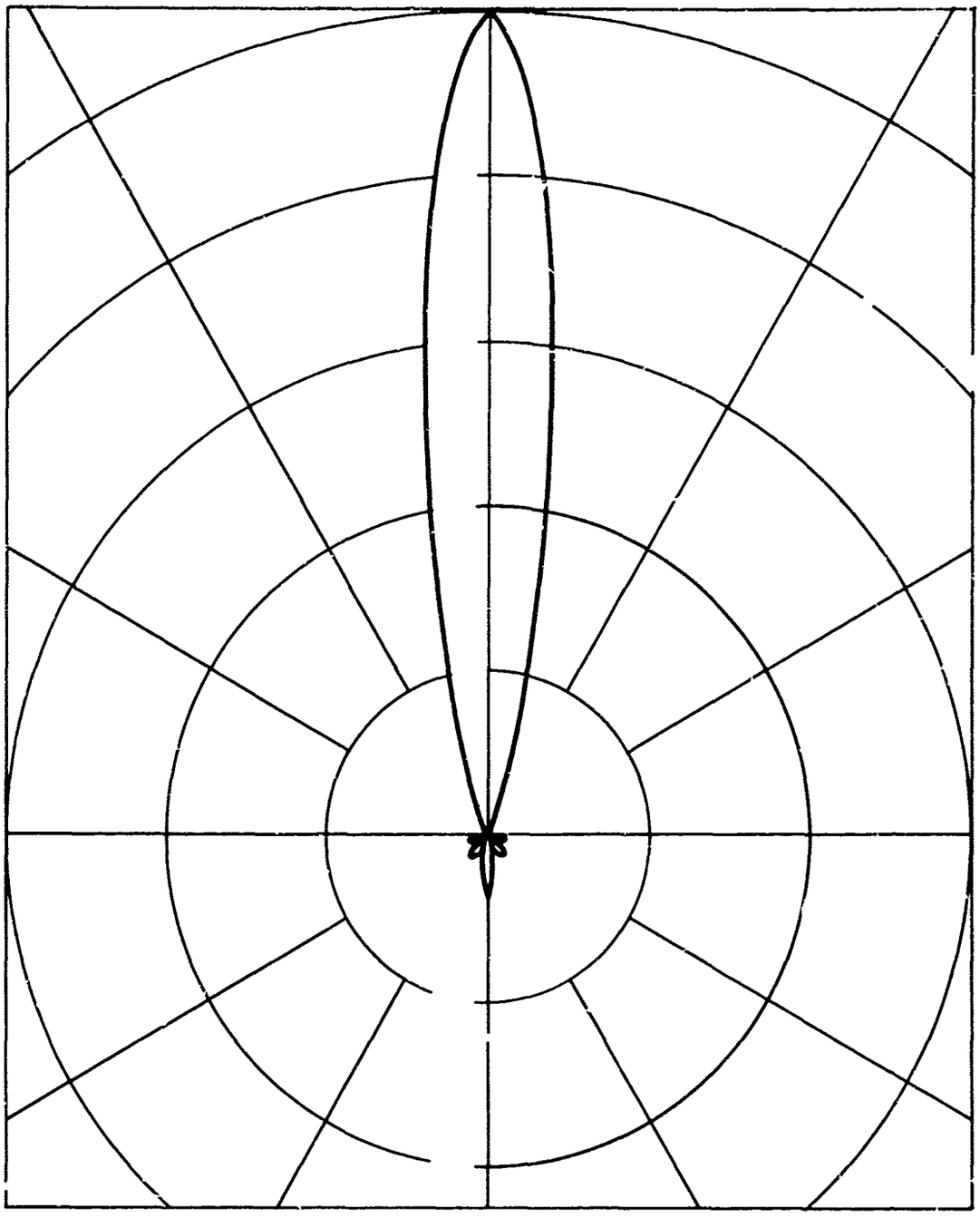

FIG. 9c: The radiation patterns of the triangular lattice arrays with $d/\lambda = 0.8$, $h/\lambda = 0.4$, E-plane pattern of a 15-element short dipole array.

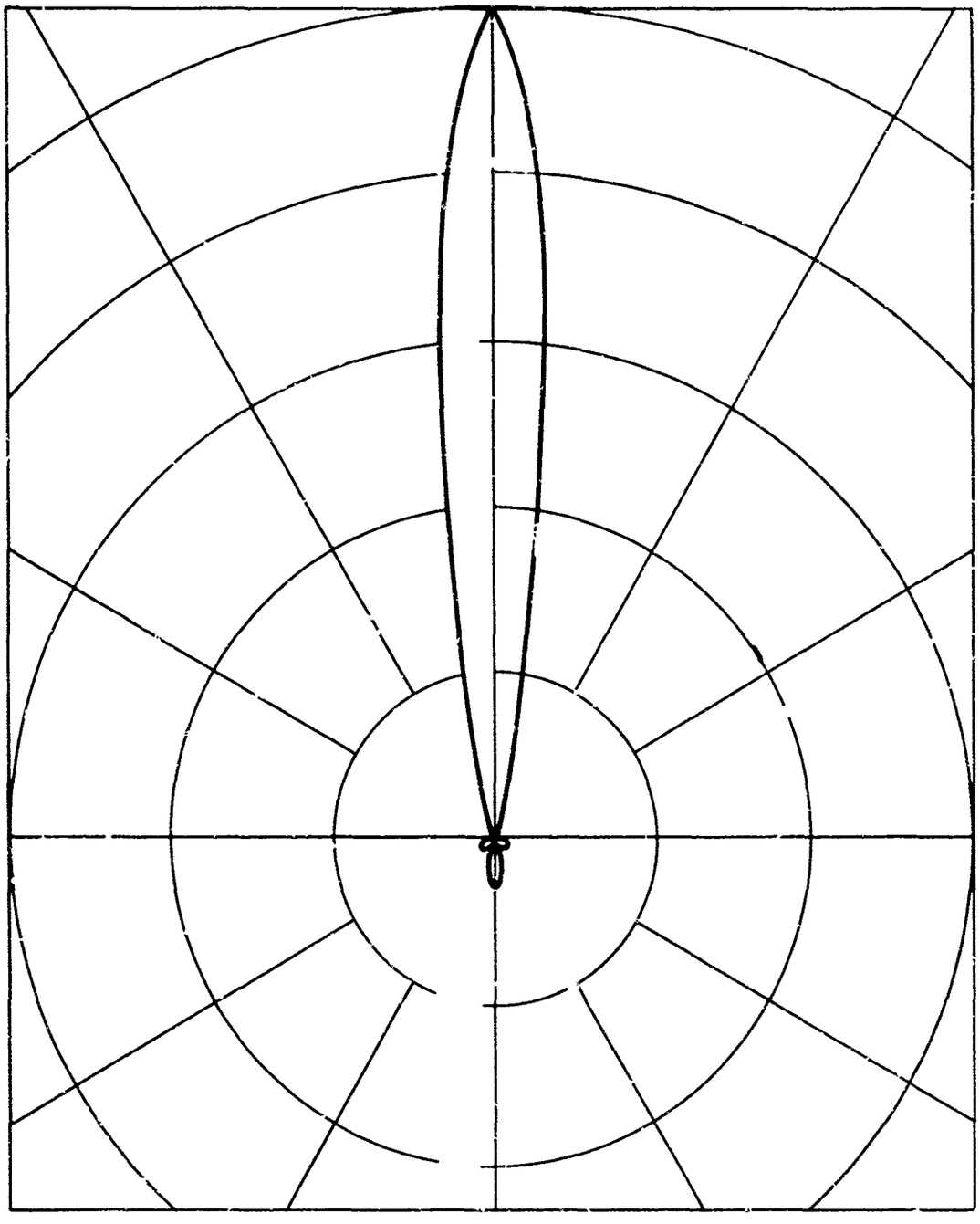

FIG. 9d: The radiation patterns of the triangular lattice arrays with $d/\lambda = 0.8$, $h/\lambda = 0.4$, E-plane pattern of a 21-element short dipole array.

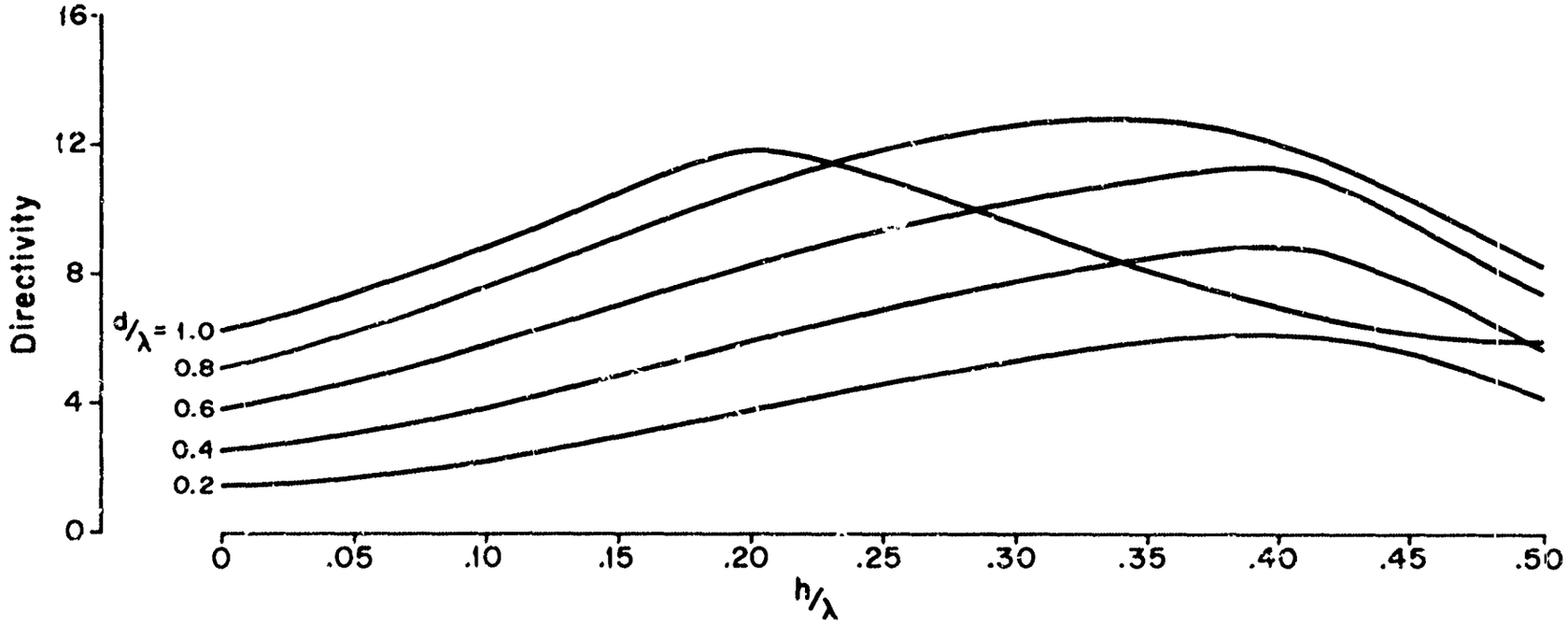

FIG. 10a: Maximum nominal directivity vs. row spacing, h/λ, with various values of element spacing d/λ, 10-element isotropic array.

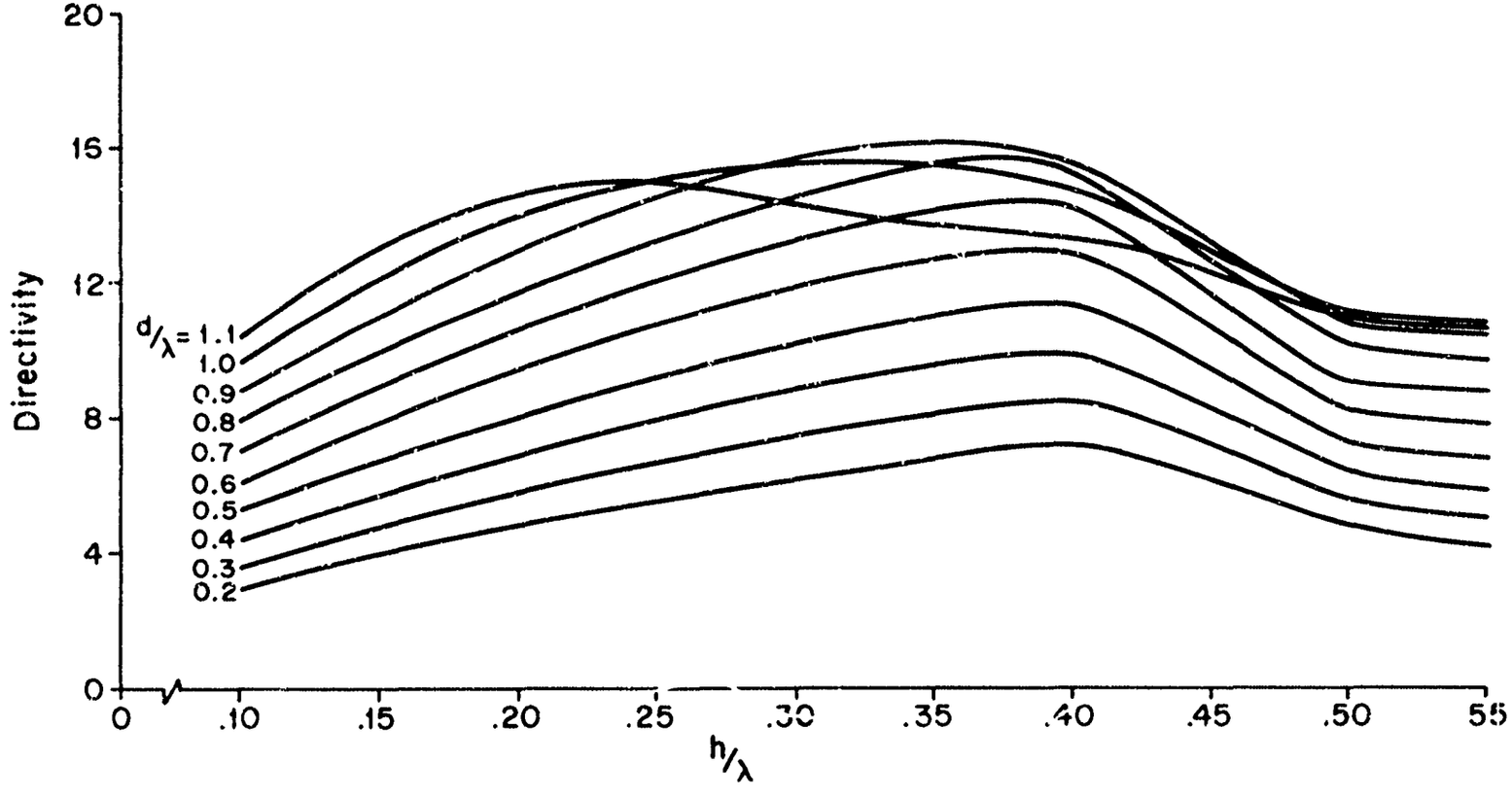

FIG. 10b: Maximum nominal directivity vs. row spacing, h/λ, with various values of element spacing d/λ, 10-element short dipole array.

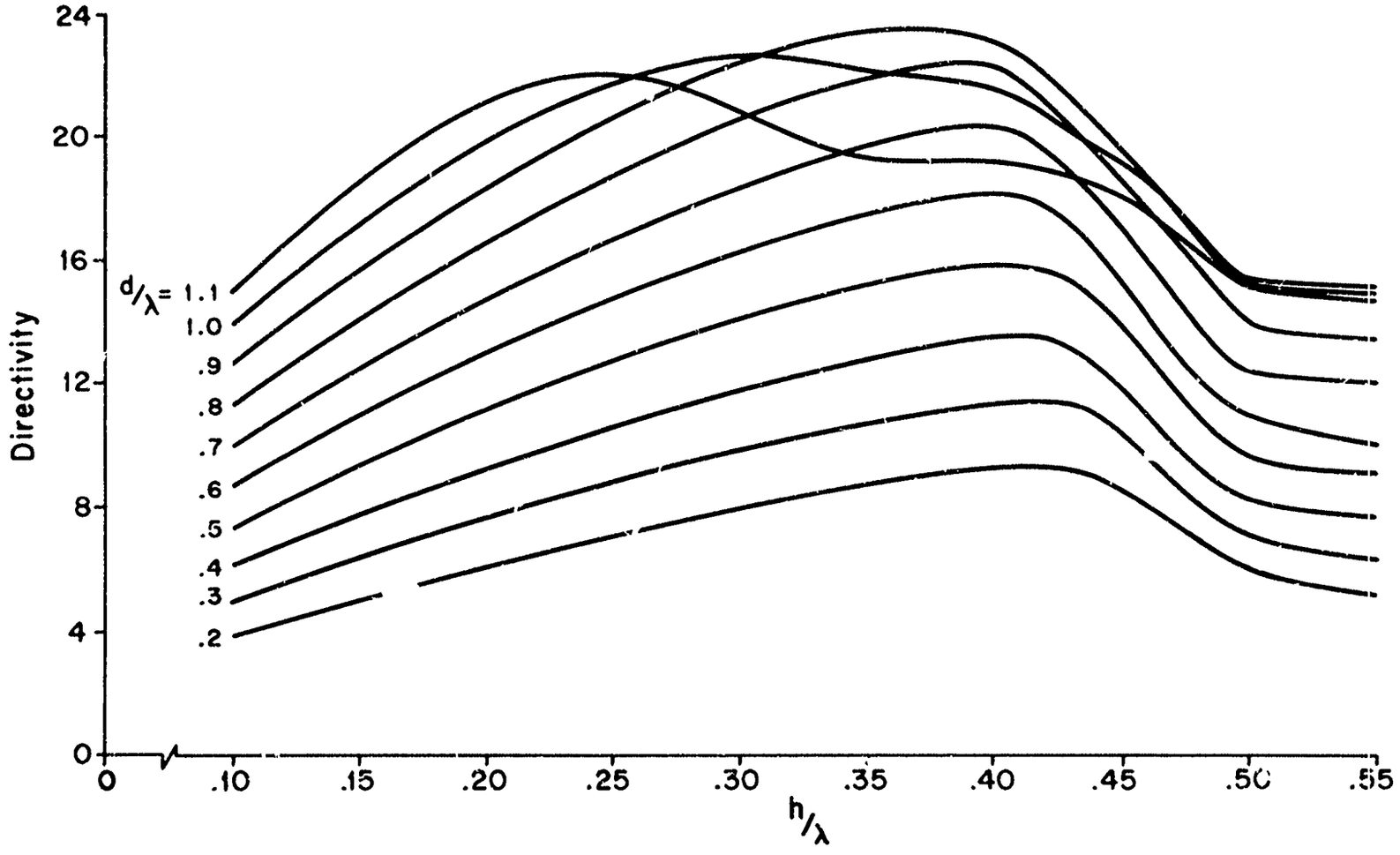

FIG. 10c: Maximum nominal directivity vs. row spacing, h/λ, with various values of element spacing d/λ, 15-element short dipole array.

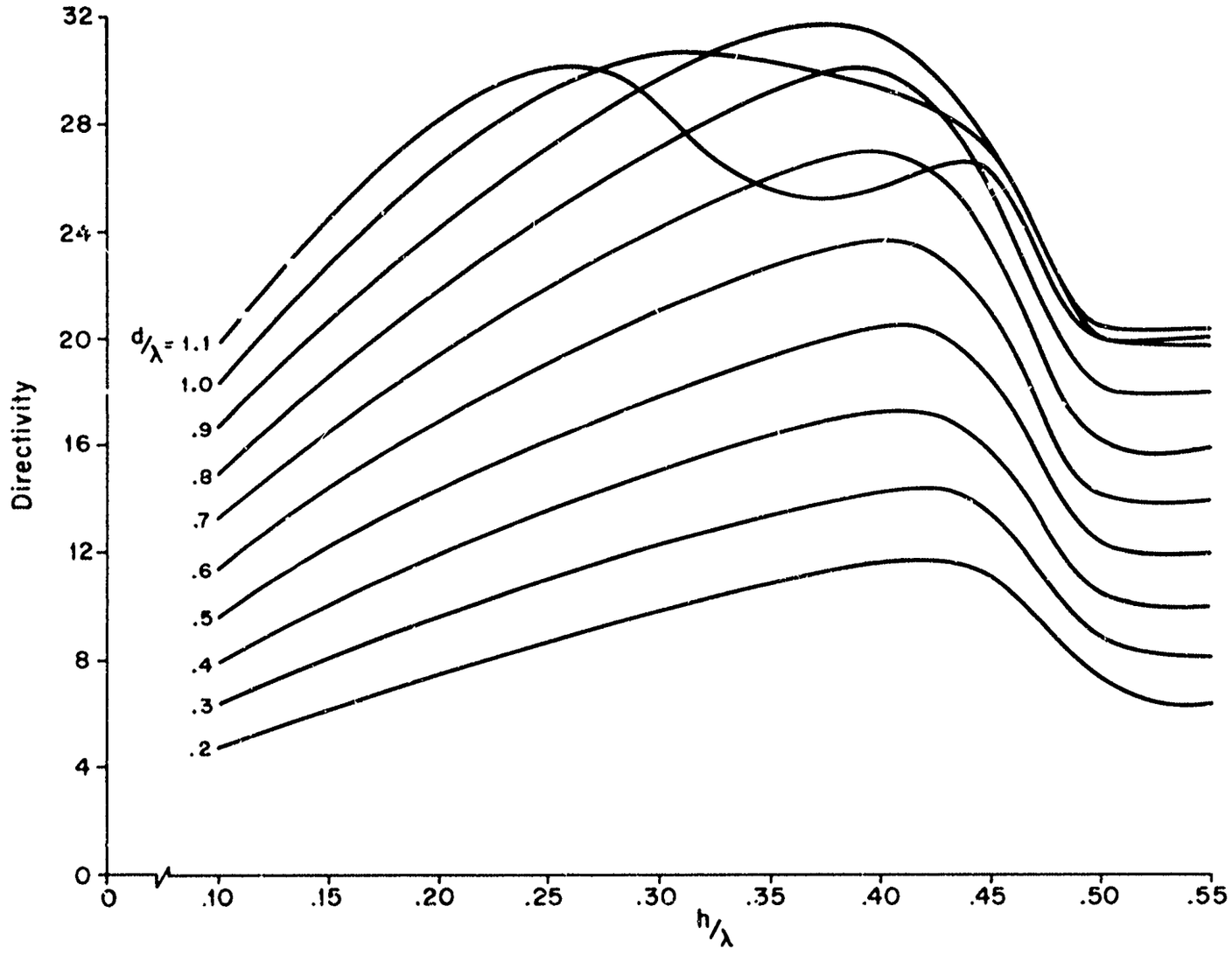

FIG. 10d: Maximum nominal directivity vs. row spacing, h/λ, with various values of element spacing d/λ, 21-element short dipole array.

As a function of d the directivity seems to reach a maximum in the neighborhood of d=0.9λ. This is also observed in the linear arrays (Tai,1964). The directivity of the dipole case is in general higher than that of the isotropic case. In either case, they are numerically greater than the number of elements in the array.

VII

CONCLUSION

Because of the symmetry involved in the structure of the array, the H-plane pattern is found to depend only on the row spacing. It is much broader than the E-plane pattern. The E-plane patterns indicate that the main beam becomes sharper at the expenses of the emerging side lobes and back lobes as the element spacing becomes larger. The tapering effect which is inherent in the triangular lattice configuration is rather evident.

The maximum nominal directivity seems to occur at the row spacing about 0.35λ and the element spacing about 0.9λ. This latter criterion (d=0.9λ) is also observed in the linear arrays.

In this report the numerical examples are presented only for the case where $\delta = -kh$, or the main beam is directed at $\theta_0 = 90^\circ$ and $\phi_0 = 90^\circ$. Under this case, the back lobe levels of the dipole case are the same as in the isotropic case.

As a sequel of this study, it would be interesting to extend the present work to the following:

1) The beam steering properties of the triangular lattice arrays.
2) The size of the back lobe as a function of the steering angle.
3) The rhombic array which is simply a juxtaposition of two triangular lattice structures.
4) The lattice structures on curved surfaces, such as on a section of a cone, or a section of a sphere.
5) Three-dimensional triangular array, such as pyramids or tetrahedra.

REFERENCES

Papas, C.H., Theory of Electromagnetic Wave Propagation, pp. 76-77, McGraw-Hill Book Company, New York, 1965.

Tai, C-T., "The Optimum Directivity of Uniformly Spaced Broadside Arrays of Dipoles," IEEE Trans. on Antennas and Propagation, AP-12, No. 4, pp.447-454, July 1964.

Unclassified
Security Classification

DOCUMENT CONTROL DATA - R&D

(Security classification of title, body of abstract and indexing annotation must be entered when the overall report is classified)

1. ORIGINATING ACTIVITY (Corporate author) University of Michigan	2a. REPORT SECURITY CLASSIFICATION Unclassified 2b GROUP NA

3. REPORT TITLE
PROPERTIES OF THE TRIANGULAR LATTICE ARRAY

4. DESCRIPTIVE NOTES (Type of report and inclusive dates)
Technical Report

5. AUTHOR(S) (Last name, first name, initial)
Cheng, Davis H. S.

6. REPORT DATE	7a. TOTAL NO. OF PAGES	7b. NO. OF REFS
June 1968	48p	2

8a. CONTRACT OR GRANT NO.	9a. ORIGINATOR'S REPORT NUMBER(S)
DA-ARO-D-31-124-G724 b. PROJECT NO. 20014501B31E	7678-6-T
c.	9b. OTHER REPORT NO(S) (Any other numbers that may be assigned this report) 5638.4-E
d.	

10. AVAILABILITY/LIMITATION NOTICES
This document has been approved for public release and sale; its distribution is unlimited.
Distribution of this report is unlimited.

11. SUPPLEMENTARY NOTES	12. SPONSORING MILITARY ACTIVITY
None	U.S. Army Research Office-Durham Box CM, Duke Station Durham, North Carolina 27706

13. ABSTRACT A new type of array consisting of elements arranged in a triangular lattice is studied in this report. The qrray has radiation characteristics similar to those of a tapered array but does not require tapered excitation. A phased array of an arbitrary triangular lattice configuration is formulated using the vector model. It is applied to a special case of an isosceles triangular array. The directivity of the array is derived and expressed in a compact form, whereby its enumeration becomes a routine procedure for any total number of elements. A general method of evaluating the mutual coupling terms involving two inclined short dipoles is developed. Numerical results are presented and discussed as regards the radiation patterns and directivities of an isosceles triangular lattice array with its varying parameters such as the spacings between the adjacent elements and rows of elements, the phasings of the elements, and the size of the array.

14. KEY WORDS
array
triangular lattice
vector model
isosceles triangular array
short dipoles
isisceles triangular lattice
radiation patterns

DD FORM 1 JAN 64 1473

Unclassified
Security Classification